nature ecology & evolution

ARTICLES

https://doi.org/10.1038/s41559-019-1046-4

Corrected: Author Correction

Evolution of placental invasion and cancer metastasis are causally linked

Kshitiz[1,2,3*], Junaid Afzal[4], Jamie D. Maziarz[1,5], Archer Hamidzadeh[1,2], Cong Liang[1], Eric M. Erkenbrack[1,5], Hong Nam Kim[6], Jan-Dirk Haeger[7], Christiane Pfarrer[7], Thomas Hoang[2], Troy Ott[8], Thomas Spencer[9], Mihaela Pavličev[10], Douglas F. Antczak[11], Andre Levchenko[1,2*] and Günter P. Wagner[1,5,12,13*]

Among mammals, placental invasion is correlated with vulnerability to malignancy. Animals with more invasive placentation (for example, humans) are more vulnerable to malignancy. To explain this correlation, we propose the hypothesis of 'Evolved Levels of Invasibility' proposing that the evolution of invasibility of stromal tissue affects both placental and cancer invasion. We provide evidence for this using an in vitro model. We find that bovine endometrial and skin fibroblasts are more resistant to invasion than are their human counterparts. Gene expression profiling identified genes with high expression in human but not in bovine fibroblasts. Knocking down a subset of them in human fibroblasts leads to stronger resistance to cancer cell invasion. Identifying the evolutionary determinants of stromal invasibility can provide important insights to develop rational antimetastatic therapeutics.

Placental invasion into the maternal endometrium of the uterus shows substantial similarities to early cancer dissemination into stroma[1–4]. These similarities have inspired the hypothesis of antagonistic pleiotropy[5,6]. According to this hypothesis, trophoblasts evolved the capacity to invade the endometrium, leading to invasive placentation. These mechanisms can become reactivated in cancer cells, leading to a predisposition to metastasis. This implies that cancer malignancy should be limited to placental mammals where invasive placentation first evolved. This prediction, however, is inconsistent with the fact that opossums, with ancestrally non-invasive placenta[7,8], get invasive skin cancers[9]. Here, we explore an alternative scenario in which stromal cells of the uterus evolved to either resist or permit invasion, determining the outcome of placental invasiveness[9].

The likelihood that the evolution of the stromal environment is driving the evolution of cancer malignancy is enhanced by the fact that the molecular mechanisms used by cancer cells to metastasize are shared with other biological processes. For instance, the mechanisms regulating gastrulation, wound healing, extravasation by leukocytes and so on, are shared with both trophoblast and cancer invasion[6,10,11]. This implies that invading cancer cells use mechanisms that evolved much earlier than placental invasion and, therefore, the evolution of invasive placentation per se cannot be responsible for the origin of malignant cancer. It is important to note, however, that the invasiveness of the placenta continued to evolve after its origin. Placental invasion reverted to a non-invasive phenotype in several lineages of placental mammals, as well as evolving an even higher degree of invasiveness in the great apes, which includes humans[12–14]. A complete loss of placental invasion evolved in hoofed mammals, such as cows and horses and their relatives, and these animals have lower malignancy rates for a variety of cancers[9]. In contrast, humans (with very invasive placentas) are highly vulnerable to melanoma malignancy.

On the basis of the arguments outlined above, we suggest that evolutionary changes in the permissiveness or resistance of uterine stromal cells to placental invasion are mechanistically linked to the vulnerability to cancer malignancy[9]. We term this 'Evolved Levels of Invasibility' (ELI; Fig. 1a) and experimentally test ELI using an in vitro model (Fig. 1b). We demonstrate that human fibroblasts are more permissive to invasion by trophoblasts, as well as cancer cells, compared to their bovine counterparts. We then identify factors responsible for the resistance to invasion, paving a way for therapeutic interventions. This study highlights how investigating evolutionary processes may lead to the identification of therapeutic targets, pointing to the clinical potential of evolutionary analysis.

Results

Collective cell invasion behaviour can be modelled in an ECM-mimetic co-culture system. To test ELI, we developed a method for measuring collective cell invasion into a lawn of stromal cells. The collective cell invasion into stroma is a complex process[15–17]. During infiltration and spread, invading cells interact with stroma, which modulates their invasive capacity while experiencing contact guidance from the underlying extracellular matrix (ECM) fibres[1,18,19]. On the basis of these considerations, we sought to mimic the stromal invasion process through a patterned

[1]Yale Institute of Systems Biology, Yale University, West Haven, CT, USA. [2]Department of Biomedical Engineering, Yale University, New Haven, CT, USA. [3]Department of Biomedical Engineering, University of Connecticut Health Center, Farmington, CT, USA. [4]Department of Medicine, University of California San Francisco, San Francisco, CA, USA. [5]Department of Ecology and Evolutionary Biology, Yale University, New Haven, CT, USA. [6]Center for BioMicrosystems, Korea Institute of Science and Technology, Seoul, South Korea. [7]Institute of Anatomy, University of Veterinary Medicine, Hannover, Germany. [8]Department of Animal Science, Center for Reproductive Biology and Health, Penn State University, University Park, PA, USA. [9]Division of Animal Sciences, University of Missouri, Columbia, MO, USA. [10]Cincinnati Children's Hospital and Medical Center, Cincinnati, OH, USA. [11]Baker Institute for Animal Health, College of Veterinary Medicine, Cornell University, Ithaca, NY, USA. [12]Department of Obstetrics, Gynecology and Reproductive Sciences, Yale Medical School, New Haven, CT, USA. [13]Department of Obstetrics and Gynecology, Wayne State University, Detroit, MI, USA. *e-mail: kshitiz@uchc.edu; andre.levchenko@yale.edu; gunter.wagner@yale.edu

co-culture of stromal and invasive cells on structured adhesion substrata. This approach was validated in previous cancer–stroma interaction studies[20,21]. The extent of invasion was measured as the average distance over which invasive cells have penetrated the stromal monolayer. The platform also enabled the sensitive measurement of cell invasion (Fig. 1c).

We first compared the spread of malignant (1205Lu) and non-malignant (WM35) melanoma cells into a monolayer of human skin fibroblasts (BJ5ta) on substrata reproducing the nanotopographic features of aligned ECM fibres or on flat surfaces. Aligned matrix fibres are a common feature in many tissues[22]. We found that mimicking aligned ECM matrix microenvironment allowed malignant 1205Lu melanoma cells to more extensively invade the skin fibroblast monolayer than non-malignant WM35 cells did (Fig. 1d,e and Extended Data Fig. 1a). Furthermore, when 1205Lu and WM35 cells were compared on a flat surface, no statistically significant difference could be detected. In contrast, a significant difference between 1205Lu and WM35 was detectable in the ECM-mimetic platform (Fig. 1e and Extended Data Fig. 1b,c), indicating that this assay has higher sensitivity in measuring stroma invasion compared to experiments on a flat surface.

Bovine endometrial stroma is resistant to trophoblast invasion. To explore the causes of species differences in placental invasion, we measured the invasion of a human choriocarcinoma (J3) cell line into human endometrial stromal fibroblasts (hESFs) and compared them to bovine trophoblasts (F3) invading bovine endometrial stromal fibroblasts (bESFs). At 48 h J3 cells invaded deeply into hESF layer, while the F3 invasion into bESFs was much more limited (Fig. 1f,g and Supplementary Videos). Upon closer inspection we found that human J3 cells formed invasive forks which propelled invasion into hESFs, while the bovine F3 showed no invasive forks (Fig. 1f–h). These results recapitulate the in vivo species differences during embryo implantation[23–26].

In human placenta, extravillous trophoblasts (EVTs) constitute the most invasive cell type[27,28]. We therefore measured the invasion of human chorioblastoma cell line BeWo, the EVT cell line HTR8 and the bovine F3 cells invading the layer of human or bovine stromal fibroblasts in all combinations (Fig. 2a). BeWo cells, although being a carcinoma cell line, have been extensively used as model of human cytotrophoblast cells[29]. The results showed that, while hESF were invaded by all trophoblast cell lines, both human and bovine, bESF were more resistant to invasion (Fig. 2b). The largest differences were found in the case of F3 invasion; with F3 invading rapidly into hESF monolayers but being nearly completely halted by bESFs. These cross-species invasion experiments confirmed that the limited invasion in bESF is, to a large extent, a property of the stroma cells rather than the trophoblast cells (Fig. 2b). In summary, the degree of trophoblast invasion is mostly controlled by the identity of the stromal cells rather than the invasive capacity of trophoblast cells, as assumed for ELI.

Bovine skin fibroblasts resist melanoma invasion. The findings above leave open the possibility that the observed effects could be specific to the fetal–maternal interface rather than reflecting species differences in stromal invasibility in general. In humans, melanoma invasion into the surrounding stroma is a strong predictor of malignancy[30]. Would stromal compartments in other tissues than the uterus (for example, the skin) show similar species-dependent properties to the uterine stromal cells? To address this question, we investigated whether gene expression profiles of human and bovine skin fibroblasts are more similar to those of their corresponding endometrial fibroblasts in the same species than they are to their homologous cell type in the other species.

The null hypothesis of independent transcriptome evolution of cell types predicts that corresponding (homologous) cell types should be more similar to each other than they are to a different cell type in the same species[31]. This is because, for instance, the human and bovine lineages diverged more recently than skin and endometrial fibroblasts have differentiated in evolution. This is necessarily true because otherwise corresponding cell types would not be homologous[32]. On the other hand, if gene expression profiles in skin and endometrial fibroblasts co-evolved, the cells from the same species could be more similar than to the corresponding/homologous cell in the other species. ELI predicts that, in each species, endometrial fibroblasts and skin fibroblasts share the same level of invasion resistance because their gene expression profiles co-evolved, such that selection for higher or lower endometrial invasiveness has a parallel effect on the invasibility of skin fibroblasts. Therefore, we expect that the stromal cell types from the same species are more similar to each other than they are to corresponding cell types in the other species[33].

To evaluate this expectation, we performed RNA sequencing on bovine and human skin fibroblasts and compared them to human and bovine endometrial fibroblasts. Principal component analysis showed that the gene expression distance between skin fibroblasts and endometrial stromal fibroblasts of the same species was less than the distance between corresponding cell types of different species (Fig. 2c). The observed pattern is consistent with the suggestion that gene expression in endometrial and skin fibroblasts indeed co-evolved due to pleiotropic effects of mutations on transcriptional regulation[31,33]. In other words, the biology of skin and endometrial fibroblasts can be expected to be similar within species even though they differ between species.

We then measured invasion of malignant human melanoma cells (A375) into the skin fibroblasts from human (BJ5ta) and bovine (bSkFb) and found that bSkFb indeed resisted A375 invasion more strongly than did human skin fibroblasts (Fig. 2d). This greater invasion resistance of bSkFb was supported by a similarly

Fig. 1 | An experimental platform to test ELI. a, Illustration of ELI. Placentation in humans is haemochorial, where the placental trophoblasts invade the maternal stroma reaching the blood supply. In contrast, in cows and other boroeutherians, placentation has recently evolved to be epitheliochorial, where the trophoblast epithelium attaches to the endometrial epithelium but does not invade the maternal interstitium. The ELI suggestion is that bovine stroma has evolved to resist invasion compared to human stroma and, therefore, secondarily limits cancer metastasis. **b**, Illustration showing a cell-patterning nanotextured platform to quantitatively and sensitively measure collective invasion into stroma; stromal cells and invasive cells are patterned by a PDMS stencil into juxtaposed monolayers heterotypically interacting with each other, and imaged using live-cell microscopy to observe collective cell invasion into the stroma. **c**, Time-course images showing invasion of 1205Lu malignant melanoma cells (red) into BJ5ta human skin fibroblasts (unlabelled) for 18 h on a flat substrate versus a nanotextured substrate. **d**, Quantification of the extent of invasion per unit length of heterotypic intercellular interaction. **e**, Quantification of the extent of invasion of non-malignant WM35 and malignant 1205Lu melanoma into a monolayer of BJ5ta human skin fibroblasts on flat and nanotextured substrata. **f**, Time-course images showing invasion of human choriocarcinoma-derived trophoblasts, J3 (red), into human endometrial stromal fibroblasts (unlabelled); and bovine trophoblasts, F3 (red), into bovine stromal fibroblasts (unlabelled) for 48 h. See Extended Data Fig. 2 for phase contrast and Supplementary Videos for dynamics of invasion. **g**, Quantification of the extent of invasion of trophoblasts into the respective stromal monolayer. **h**, Time-course dynamic analysis showing cumulative invasion of J3 and F3 into respective species-specific endometrial stromal monolayers. In **d**, **e** and **g**, $n = 4$ independent biological replicates. Statistical comparisons made using Student's *t*-tests $^{**}P < 0.01$, $^{***}P < 0.001$; error bars denote s.e.m.; NS, not significant.

high resistance of these cells to invasion by WM35, 1205Lu and SKMel28 melanoma cell lines (Fig. 2e). A similar assay with bovine melanoma cells was precluded owing to lack of bovine melanoma cell lines[34]. Overall, these results indicate that bovine skin fibroblasts can resist cell invasion better than their human counterparts can.

Human and bovine fibroblasts respond differently to trophoblast co-culture. To understand the genetic underpinnings of ELI in bovine stromal cells, we collected RNA sequencing data from human and bovine endometrial fibroblasts, with and without co-culture with the respective trophoblasts. We focused on differentially

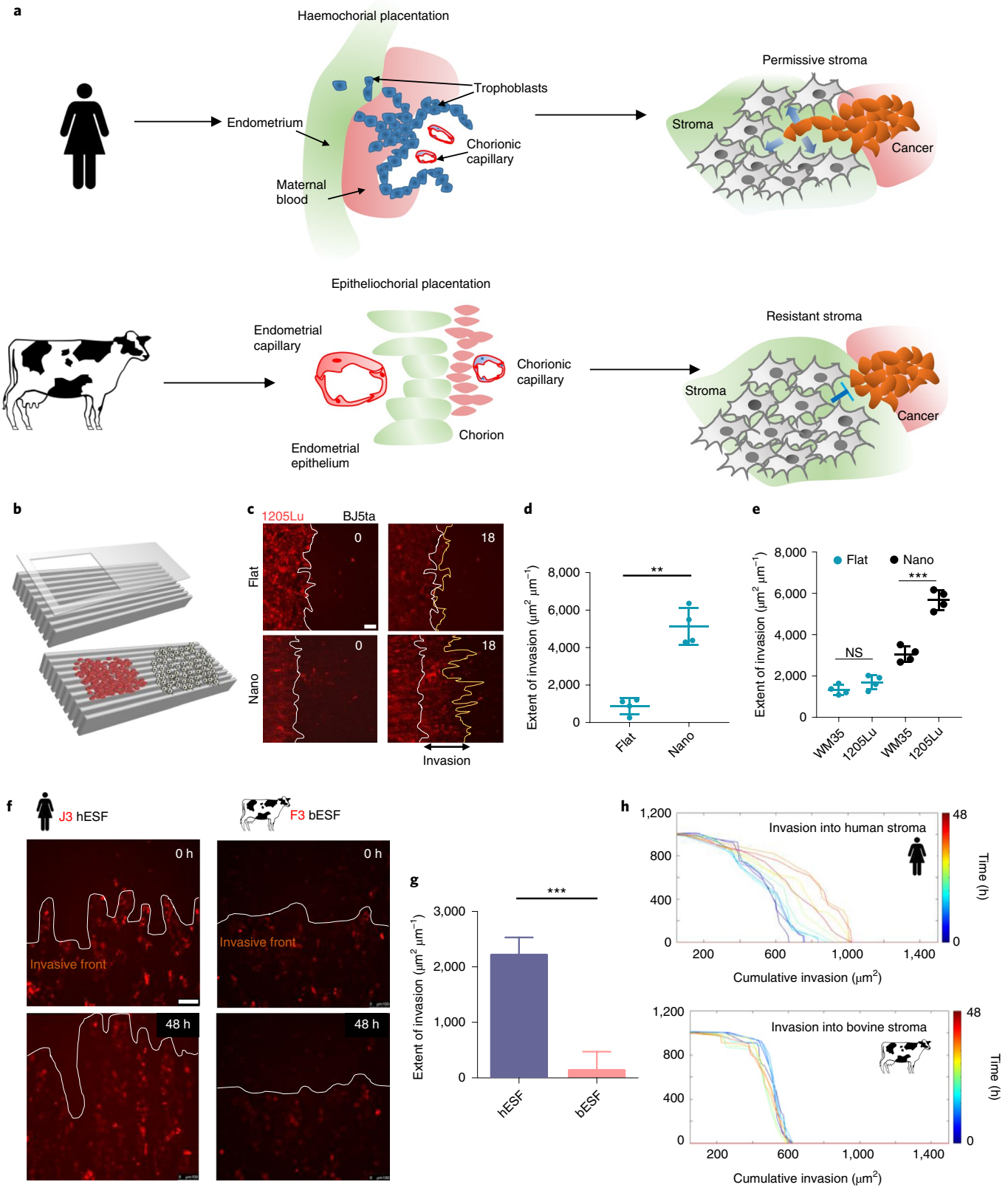

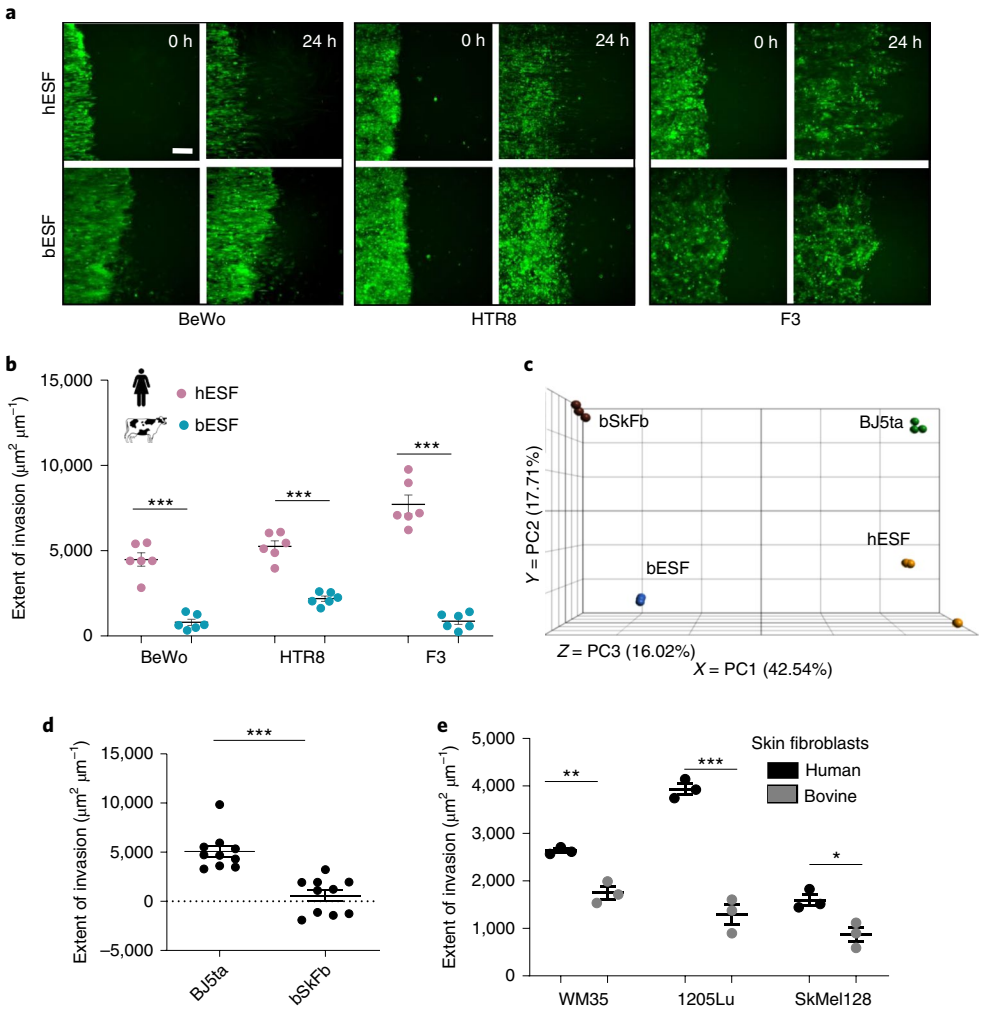

Fig. 2 | Bovine stroma resists trophoblast and melanoma invasion. a, Representative time-course images of human trophoblasts BeWo, extravillous trophoblasts HTR8 (green) and bovine trophoblasts F3 (green) invading ESF of the respective species for 18 h. White traces show the boundary of the invasive fronts. **b**, Quantification of the extent of invasion for either trophoblasts. **c**, Principal component (PC) analysis of the gene expression data from skin fibroblasts from human (BJ5ta) and bovine (bSkFb) and ESFs from human (hESF) and bovine (bESF); three biological replicates were used for RNA sequencing. **d**, Extent of invasion of malignant A375 cells into BJ5ta and bSkFb monolayers measured over 24 h. **e**, Extent of invasion of other well-characterized human melanoma cell lines into BJ5ta and bSkFb monolayers after 18 h of observation. In **b**, **c** and **e**, $n=3$ and in **d**, $n=8$ independent biological replicates; statistical comparisons made using Student's *t*-tests $^{*}P<0.05$, $^{**}P<0.01$, $^{***}P<0.001$; error bars denote s.e.m.

expressed genes in stromal cells, both basally and upon interaction with species-specific trophoblasts. Endometrial fibroblasts of both species were labelled with DiI fluorescent stain and co-cultured with equal number of unlabelled trophoblast cells, HTR8 and F3 for human and bovine cells respectively (Extended Data Fig. 3a). Co-cultures were maintained for 72 h and the cells were sorted using fluorescence-activated cell sorting (FACS)[20]. Henceforth, the bovine cells will be referred to as bESFs and bESF$^{co\text{-}F3}$ and human cells as hESFs and hESF$^{co\text{-}HTR8}$.

Many genes were differentially expressed in bovine versus human endometrial fibroblasts (Extended Data Fig. 3b) and ESFs responded strongly to co-culture with their cognate trophoblasts cells (Extended Data Fig. c,d). Furthermore, human and bovine ESFs responded differently to trophoblast co-culture (Fig. 3a,b and Extended Data Fig. 3e,f). Human and bovine endometrial stromal cells differed substantially with respect to the number of genes affected by co-culture, with human cells showing more differentially expressed genes (5,349 genes changed at $P\leq0.01$; false discovery rate, FDR$=3.1\times10^{-3}$) compared to bovine cells (3,101 genes at $P\leq0.01$; FDR$=7.01\times10^{-3}$). Gene-set analysis revealed genes belonging to chemotactic activity, cell motility and metastasis ontologies at higher relative abundance in hESF$^{co\text{-}H8}$ compared to bESF$^{co\text{-}F3}$ (Fig. 3b). These results suggest that species differences in invasibility may be caused by differential gene expression among the stromal cells in response to trophoblast cells.

We found that human and bovine ESFs expressed markedly different sets of chemokine ligands (Fig. 3c) and chemokine receptors (Fig. 3d), although both were enriched in transcripts associated with angiogenesis. Genes showing elevated expression in hESFs included fibroblast growth factors, vascular endothelial growth factors, semaphorins, members of the transforming growth factor (TGF) family, as well as NRPs and *ROBO1*, whereas bESFs showed high expression of endothelin (*END1*), plasminogen activator (*PLAU*), thrombopoeitin (*THPO*) and notably, transforming growth factor β2 (*TGFB2*). In contrast, genes belonging to ontologies GO_adherens junction and endothelial barrier did not show systematic expression differences in favour of either hESF or bESF (Extended Data Fig. 4a,b). Finally, the genes related to GO_fibroblast migration tend to be expressed at lower levels in bESF versus hESF (Extended Data Fig. 4c). These data point to the possibility that stromal response to

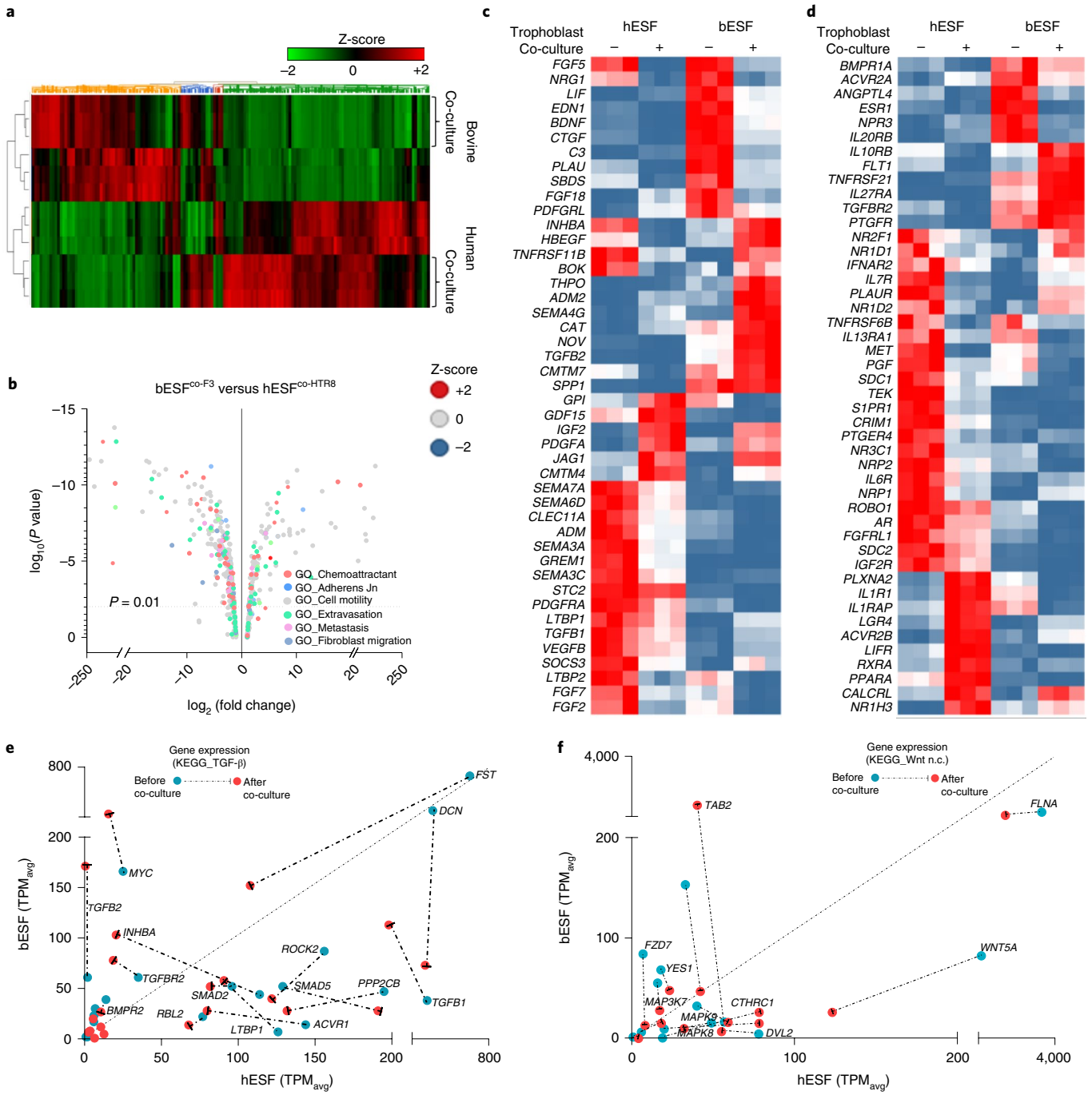

Fig. 3 | Transcriptomic analysis of bovine and human ESFs reveals differential response to trophoblasts. a, Heatmap of gene expression differences of human and bovine ESFs with and without co-culture with HTR8 and F3 trophoblast cells, respectively. **b**, Volcano plot showing fold differences in the TPM values of bESFs versus hESFs co-cultured with the respective trophoblasts, colour-coded for relevant gene ontologies. **c**,**d**, Heatmaps showing expression of genes in hESFs and bESFs with or without co-culture with HTR8 and F3, respectively, belonging to the gene-sets chemokine (**c**) and chemokine receptors (**d**). **e**,**f**, TPM values of genes significantly different in hESFs and bESFs for KEGG pathways for TGF-β (**e**) and non-canonical WNT signalling (**f**). For each gene, TPM values before and after co-culture are shown as blue and red dots, respectively. Arrows show the change in TPM values due to trophoblast co-culture.

trophoblast co-culture varies strongly between the species for genes that could play a role in the interaction between invading trophoblast cells and stromal cells, as opposed to genes that regulate basal stromal integrity. Differential expression of these genes may affect the invasibility phenotype in either species.

These analyses suggested that differences in the interactions between the stromal and invading cells were drivers of ELI in human and bovine. For instance, transforming growth factor β (TGF-β) and WNT signalling pathways are mediators of cancer stromal interaction[35–40] and thus we explored the effect of trophoblast co-culture on the activation of these signalling pathways to see whether there are parallels between cancer–stroma and trophoblast–endometrial stroma interactions. Expression of genes in non-canonical WNT and TGF-β pathways were indeed higher in

hESFs compared with bESFs (Fig. 3e,f). Ingenuity pathway analysis showed that both signalling pathways were differentially activated in bovine and human ESFs (Extended Data Fig. 4e). Although co-culture with trophoblasts resulted in reduction in expression of genes belonging to TGF-β pathway for hESFs, they continued to remain many times higher when compared in bESFs. While TGF ligands *TGF-β1* and *TGF-β3* as well as receptors of the TGF-β family (for example, *ACVR1*) were highly expressed in hESFs, negative regulators like *TGF-β2* and *inhibin-A* were expressed at higher levels in bESFs. Similarly, we observed that downstream transcription factors *SMAD-2*, *-3* and *-5*, as well as the co-SMAD, *SMAD4*, were expressed at higher levels in hESFs compared to bESFs (Fig. 3e). Similarly, many members of the WNT signalling network showed higher expression in hESF versus bESF (Fig. 3f and Extended Data Fig. 4d). These results supported a role for paracrine signalling between heterotypic cells during the invasion processes in both the uterus and in tumour lesion, prompting us to further explore the role of the signalling networks in stromal invasion.

Selected gene knockdown in human fibroblasts increases resistance to melanoma invasion. We hypothesized that modulating the differentially expressed genes in human stromal cells could induce them to become more resistant to invasion in human cells. We focused on genes related to WNT and TGF-β signalling. Specifically, we selected 16 genes from the TGF-β and WNT pathways that had higher expression in hESF or were upregulated in hESF in co-culture with trophoblast cells (Fig. 4a). We then targeted these genes using a battery of small interfering RNAs (siRNAs) in hESFs and BJ5ta to test whether they could modulate stromal invasibility.

Comparison of each siRNA-transfected stromal cell population was made with appropriate untransfected controls, as well as with cells transfected with control non-targeting siRNA (Extended Data Fig. 5a,b). HTR8 invasion into hESF was significantly reduced after 24 h in eight out of 16 genes (Fig. 4b). A375 invasion into BJ5ta skin fibroblast monolayer was observed for 18 h and 36 h after gene knockdown. Nine of these gene knockdowns significantly decreased invasion into the skin fibroblast monolayer (Fig. 4c), including members of WNT superfamily, TGF-β ligands, as well as less-established targets and effectors of WNT signalling, for example *STARD7* (ref. [41]), *LPIN1* (refs. [42–46]) and *YAP1* (ref. [47]). Furthermore, we detected a weak but significant correlation in the increase of stromal resistance to invasion following gene knockdowns in both hESF and BJ5ta ($R^2 = 0.25$, $P = 0.02$), indicating that gene silencing enhances resistance to invasion in a similar manner in both human endometrial and skin fibroblasts (Fig. 4d). Moreover, the average response for all gene knockdowns was an increase in resistance to invasion (Fig. 4e). These results suggested that human skin fibroblasts could be induced to resist melanoma invasion and that knowledge of gene expression in cow fibroblasts can tell us how to achieve this.

Opposite evolutionary trends of vulnerability to malignancy in humans and bovines. To assess the evolutionary history of the expression of the genes identified above as important for ELI, we cultured the ESFs from rabbit, rat, guinea pig, cat, horse and sheep to extend our analysis (Fig. 4f). This taxon sample represents two clades of eutherian mammals, the Euarchontoglires and the Laurasiatheria, together forming the clade of Boreoeutheria. We plotted the phylogenetic tree of these eight species[48], along with the expression of these genes in skin fibroblasts compared to the inferred boreoeutherian ancestor ($\sqrt{\text{TPM}_{\text{species}}} - \sqrt{\text{TPM}_{\text{ancestor}}}$, where TPM is transcripts per million).

We found, surprisingly, that humans evolved higher expression levels of invasibility enhancing genes (*TGFB1, ACVR1, DDR2, LPIN1, CD44, MMP1*), compared to the inferred boreoeutherian ancestor. The expression levels of these genes in human skin fibroblasts is higher than that of rabbit, rat and guinea pig. All of these species have haemochorial placentation and, thus, the higher expression level of these genes in humans probably evolved in the primate lineage. The limited data on a selected group of genes, therefore, supports ELI amongst mammals and points to the possibility of increased stromal vulnerability in humans and decreased stromal vulnerability in bovines.

Discussion

Mammalian species differ in their potential for tumourigenesis, as well as their vulnerability to cancer metastasis[9,49]. The comparative biology of cancer incidence across different animals has identified species-specific tumour suppressor mechanisms explaining the variation in occurrence of tumours between species[50–55]. In a recent review, Constanzo and collaborators made a convincing case for a model where cancer progression in humans includes the reactivation of embryonic gene expression normally controlling placenta development and immune evasion[56]. Here, we focus on differences across species in the rates of cancer malignancy rather than differences in rates of tumourigenesis. For instance, melanoma does occur in bovines and equines but remains largely benign[57–59]; while it is highly malignant in humans. This correlates with the phenotype of the fetal–maternal interface (the degree of placental invasion during pregnancy).

In human stromal fibroblasts, siRNA-guided knockdown revealed genes that impart stromal invasibility by melanoma and trophoblast cells (Fig. 4g). These genes include TGF-β ligands, consistent with results from colorectal cancer[38]. Other genes enhancing stromal invasibility are members of the non-canonical WNT pathway, as well as WNT signalling modulators (for example, *LPIN1*, ref. [60]), by directly regulating β-catenin levels (for example, *YAP/TAZ*, ref. [47]) or by being regulated by β-catenin-induced transcription (for example, *CD44*, ref. [61]). Of these, *YAP1*, a Hippo signalling pathway target promoting tumour growth[62], can also be regulated by non-canonical WNT signalling and can, in turn, inhibit canonical WNT signalling[47]. Both TGF-β[63,64] and non-canonical WNT signalling[65,66] are known to affect tumour progression and metastasis. TGF-β1 and TGF-β3, expressed at relatively higher levels in hESF, are also reported to regulate β-catenin activity, indicating that human stromal vulnerability to invasion may be influenced by paracrine signalling to invading cells through secreted ligands. Also of interest, many of the genes identified in our comparative gene expression screen have connections to metabolic regulation. These include genes encoding LIPIN1, which regulates triglyceride metabolism[67], and MGAT5, known to regulate glucose uptake in tumour cells[68].

The results presented here show that species differences in malignancy rates may, in part, be caused by species differences in invasibility of stromal cells. We found that bovine stroma evolved lower invasibility probably via decreased paracrine signalling through TGF-β and WNT pathways. In particular, these results argue that TGF-β secretion and high non-canonical WNT signalling in stromal cells are causal factors explaining the high vulnerability of human stromal tissues to cancer invasion, at least in the case of melanoma. Comparative transcriptomic data across multiple additional species further suggests that the human lineage evolved higher expression of these genes enhancing tumour and trophoblast invasion and, thus, probably has evolved higher malignancy rates than in the common ancestor of boreoeutherian mammals.

Our data support the ELI hypothesis, suggesting that differences in stromal gene expression between species are causal in determining the degree of embryo implantation as well as stromal resistance to early cancer dissemination. In Eutheria epitheliochorial placentation has evolved several times from the pre-existing invasive placentation, suggesting that evolutionary advantages of non-invasive placentation[12–14] may drive corresponding differences in malignancy resistance. We further found that apes may also have evolved increased stromal receptivity to trophoblast invasion and

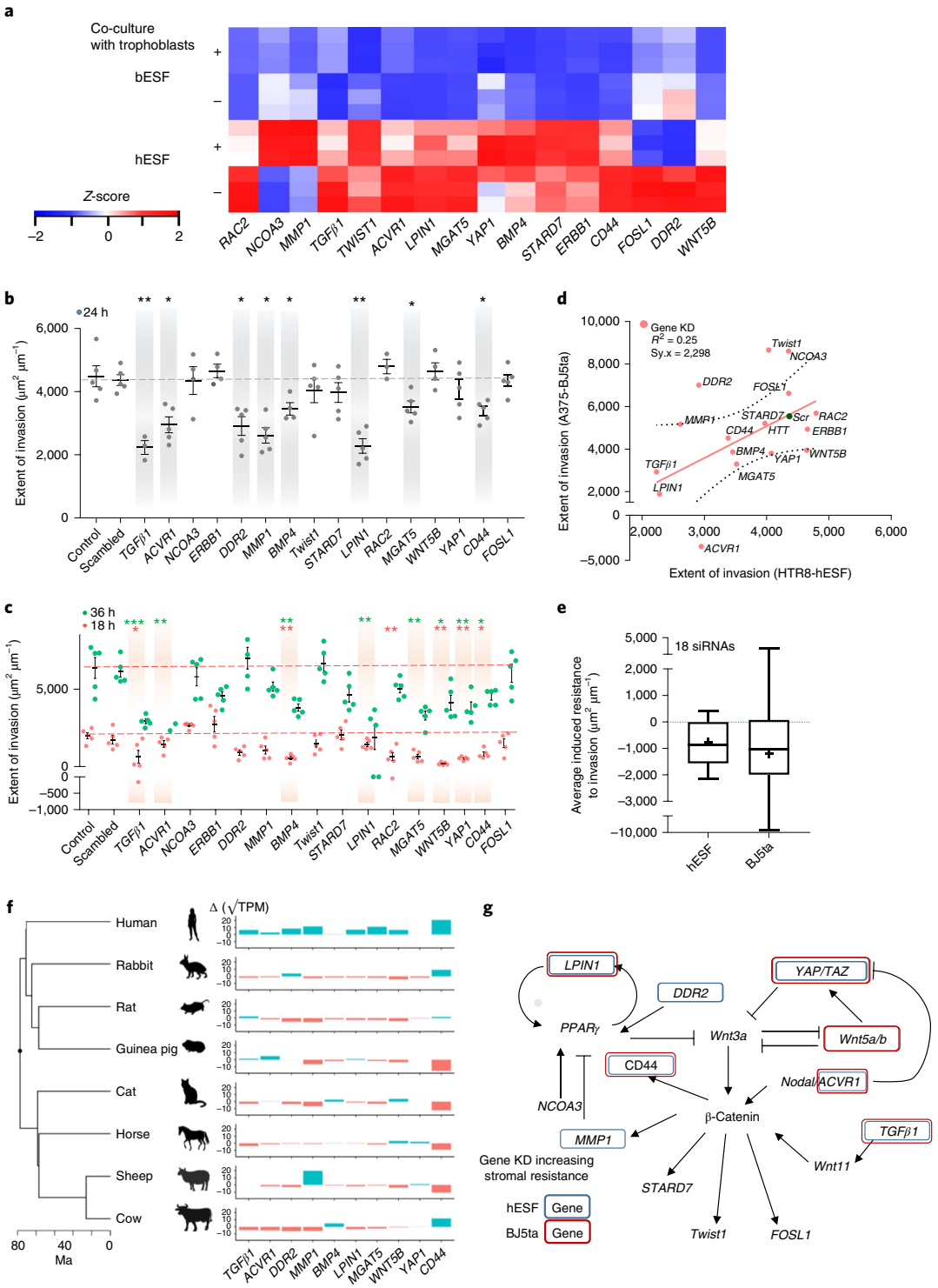

Fig. 4 | Induced resistance to invasion in human stroma by evolutionarily inspired gene silencing. a, Heatmap showing selected set of genes used for gene silencing in human stromal fibroblasts. Shown are *Z*-scores of TPM values for each transcript. **b**–**e**, siRNA-based gene knockdown in human stroma to induce expression similar to bESF increases resistance to invasion. **b**, Extent of invasion of HTR8 cells into hESFs subjected to siRNA-mediated gene silencing measured over 24 h using nanotextured platform. **c**, Extent of invasion measured for 18 h (red) and 36 h (green) using nanotextured platform for A375 invasion into BJ5ta subjected to siRNA-induced silencing of individual genes. Each dot in **b** and **c** reflects an individual invasion observation. Error bars show s.e.m. Statistical comparisons made with scrambled siRNA using Student's *t*-test: $*P<0.05$, $**P<0.01$, $***P<0.0001$. **d**, Correlation shown between the extent of invasion of HTR8 into hESF and A375 into BJ5ta for each siRNA-based gene silencing. **e**, Average extent of invasion in hESF and BJ5ta for the above 16 genes silenced normalized to the extent of invasion observed for control scrambled siRNA knockdown in either human stromal cells. Whiskers show minimum to maximum values; horizonal bar is the median; average values are indicated by +, box is 25th to 75th percentile. **f**, Relative transcript levels of the selected genes in various boroeutherian species compared to their most recent common ancestor; red-coloured bars denote decrease and blue bars show increase in $\sqrt{\text{TPM}}$ values versus the common ancestor; Ma, million years ago. **g**, Network of WNT signalling and its interaction with TGF-β pathway showing previously known interactions, mapped with the gene-silencing-induced resistance in hESF and BJ5ta stromal cells.

correlatively have evolved higher vulnerability to cancer malignancy. As EVTs have evolved recently in great apes, the endometrial stroma may also have increased invasibility to accommodate the more invasive trophoblast types[69]. Our ELI hypothesis, and its experimental validation, suggest that studying the genetic basis for evolved resistance to invasion can identify factors determining the stromal control of cancer progression and identify therapeutic targets.

Methods

Cell sourcing. The study used a variety of cell sources for comparative analyses. Human ESFs were immortalized by the Charles Lockwood laboratory and obtained from Gil Mor group[70]. The F3 cells were previously established by Pfarrer's group[71,72]. The J3, HTR8/SVNeo, BeWo and BJ5ta cells were obtained from ATCC.

Skin fibroblasts bSkFb bovine (*Bos taurus*), as well as those from guinea pig (*Cavia porcellus*), sheep (*Ovis aries*), pig (*Sus scrofa*) and rabbit (*Oryctolagus cuniculus*) were obtained from fresh skin tissue. A small piece of skin was collected, hair removed and the sample was washed in PBS buffer and cut into strips approximately 1.0 cm^2. Dermis was separated from epidermis by enzymatic digestion (30 min in 0.25% Trypsin buffer at 37 °C, followed by dissociation buffer (1 mg ml^{-1} collagenase, 1 mg ml^{-1} Dispase, 400 µg ml^{-1} DNase I) for 45 min at 37 °C). Epidermis was removed and 2 mm pieces were cut from the dermis and transferred to a 12-well plate and covered with media. Fibroblasts emerged from the explants and grew to confluency in growth media. Extra tissue was removed and cells were subcultured a few times using a cell scraper.

Bovine ESFs were obtained as follows. Uterine tissues were collected from each species and primary ESF were obtained by enzymatic digestion. Uterus fragments, 2–3 mm in size, were created using a scalpel and digested with 0.25% Trypsin–EDTA for 35 min at 37 °C, followed by dissociation buffer (1 mg ml^{-1} collagenase, 1 mg ml^{-1} Dispase, 400 µg ml^{-1} DNase I) for 45 min at 37 °C. Cell clumps were homogenized by passage through a 22-gauge syringe followed by passage through a 40-µm nylon mesh filter to remove remaining clumps. A single-cell suspension was obtained from the lysate, transferred to fresh growth medium and cultured in T25 flasks. To facilitate enrichment of fibroblasts versus epithelial cells, media were exchanged in each well after 15 min to remove floating cells that had not yet attached while stromal fibroblasts had attached. Cells were grown to confluency and sub-passaged by scraping the cells off the surface to be split into two T25 flasks. At confluency, cells were split through one more round of differential attachment. We used immunohistochemistry to test for abundance of vimentin (Santa Cruz, sc-6260) and cytokeratin (Abcam, ab9377) to validate fibroblast subtype in the isolated cells.

Isolates of hESF, bSkFb and bESFs were tested for potential mycoplasma contamination and were found to be free from it.

Cell culture. Human ESFs were grown in phenol-red free DMEM/F12 with high glucose (25 mM), supplemented with 10% charcoal-stripped calf serum (Hyclone) and 1% antibiotic/antimycotic (Gibco). Decidualization was induced in ESFs with 0.5 mM of 8-Br-cAMP (Sigma) and 0.5 mM of progesterone analogue medroxyprogesterone acetate for 96 h in DMEM supplemented with 2% charcoal-stripped calf serum (Hyclone). BJ5ta (ATCC) cells were cultured in 80% DMEM and 20% MEM supplemented with 10% FBS, 1% antibiotic/antimycotic and 0.01 mg ml^{-1} hygromycin. F3 cells were obtained from Pfarrer's group and were cultured in DMEM with high glucose supplemented with 10% FBS, 1% antibiotic/antimycotic (Gibco). J3 cells were cultured in αMEM supplemented with 10% FBS, 1% antibiotic/antimycotic (Gibco), while HTR8/SVNeo (ATCC) were cultured in RPMI-1640 supplemented with 10% FBS and 1% antibiotic/antimycotic (Gibco).

Fabrication of polyurethane acrylate mould. Photoresist was spin-coated on silicon wafers and electron-beam lithography was used to nanopattern the wafers (JBX-9300FS, JEOL). After the photoresist was developed, exposed silicon was etched by deep-reactive ion etcher (STS ICP Etcher) resulting in formation of submicrometre parallel ridges. Residual photoresist was removed using ashing and diced into silica masters for subsequent replica moulding.

Ultraviolet (UV) curable polyurethane (PUA) was dropwise dispensed onto the silicon master previously prepared and contacted with polyethylene terephthalate (PET) film. Application of UV light (wavelength $\lambda = 200–400$ nm, 100 mJ cm^{-2}) for 1 min was used to cure PUA, after which the mould was peeled off with tweezers and cured overnight under UV light to terminate the residual acrylate groups. The process resulted in a PUA mould of ~50 µm thickness.

Fabrication of nanotextured substrate. Previously prepared PET mould was used as a replica mould to transfer the topographic pattern onto glass substrate using the technique of capillary force lithography. Briefly, glass substrate was cleaned using NaOH (0.1 M for 1 h), washed with deionized water and dried under N_2 stream. Primer (phosphoric acrylate and propylene glycol monomethyl ether acetate in a ratio of 1:10) was spin-coated on the coverslip as a thin layer and baked for 20–30 min at 70 °C. Then 150 µl of PEG-DA (molecular weight = 575) precursor was dispensed dropwise onto the primed coverslip and the PET mould was placed reversibly. After the PUA precursor filled the submicrometre cavities by capillary action, the substrate was cured in UV light ($\lambda = 250–400$ nm, 100 mJ cm^{-2}) for 1 min. The mould was peeled after polymerization using tweezers. The substrate resultant from the method consisted of nanotextured grooves with an expected elastic modulus of ~70 MPa. The substrate was cured again for 1 h under UV light to terminate residual active acrylate groups.

Cell patterning for stromal invasion assay. For cell patterning, we used a stereolithographic plastic mould to create a polydimethylsiloxane (PDMS) stencil. The PDMS stencil was cast by mixing monomer and cross-linker in a ratio of 10:1 and cured at 80 °C for 4 h by placing it on a predesigned plastic mould. Stencils were washed using isopropyl alcohol and dried using N_2 stream, placed on the nanotopographic substrate coated with laminin (25 µg ml^{-1}) and the device kept in a vacuum to allow air under the stencil to be removed to avoid chance of leakage. DiI-labelled invasive cells were seeded onto the stencil at a density of 10^6 cells per 100 µl and allowed to attach and polarize for 8 h. Unattached cells were washed off twice with PBS and the stencil removed carefully using blunt-end tweezers. Unlabelled stromal cells were seeded at a density of 10^6 cells per 100 µl to attach to the area previously covered by PDMS stencil. After 6 h of attachment, unattached cells were washed off and the substrate mounted for live-cell microscopy. To ensure selection of definitive fibroblasts, and to avoid selection of trophoblasts taking up dye from dead stromal cells and occasional heterotypic cell-fusion events, we only collected DiI^{high} cells. All experiments were conducted in similar culture conditions by 1:1 mixture of the media in either comparable conditions.

Live-cell fluorescence microscopy. Phase-contrast and epifluorescence microscopy was performed using a Leica DMi8 model, with an HC PL Fluotar ×10, 0.30 dry objective and images were acquired using Leica LASX Software and processed using Fiji image analysis software. Lumencor SpectraX was used as a source of light for excitation and routed through a rhodamine excitation filter cube consisting of excitation 546 nm per 10 nm (band-pass filter), dichroic 560 nm (long-pass filter) and emission 585 nm per 40 nm (band-pass filter) and acquired using an Andor EMCCD iXon Ultra 888 camera.

Invasion analysis. Acquired sequential images for each condition were analysed using Fiji image analysis software after contrast enhancement. DiI-labelled invasive cell fronts (trophoblasts or melanoma cells) were identified manually for each time point. Area occupied by DiI-positive cells was measured at each time point. Total invasion was calculated as follows:

$$\delta\mathrm{Area}(t) = \mathrm{Area}(t) - \mathrm{Area}(t_0)$$

Extent of invasion per unit measurement of interface was determined by dividing δArea by the length of initial intercellular interface:

$$\langle\delta\mathrm{Area}(t)\rangle = \frac{\delta\mathrm{Area}(t)}{L(\mathrm{interface})}$$

Fluorescence-assisted flow sorting. Cells were detached from the substrate using TrypLE solution (Gibco), quenched with excess medium and washed thrice with PBS. Isolated cells were suspended in 1% AlbuMAX (Gibco) dissolved in PBS and sorted using FACS. FACS was performed using BD FacsARIA II using PE.Cy5 channel and analysis performed using FACSDiva v.6.0. To increase the purity of ESFs collected after the co-culture experiments and to account for possible uptake of dye from dead or dying stromal cells by the trophoblasts, as well as for occasional cell-fusion events, we only sorted DiI^{hi} cells. Sorted cells were collected directly in RNASelect to limit RNA degradation. Even cells that were not in co-culture were subjected to the same sorting protocol.

siRNA transfection and characterization. For gene-silencing experiments, stromal cells (BJ5ta or hESFs) were cultured in 12-well plates and transfected with at least two siRNAs (shown in Table 1) at a concentration of 50 nmol per well. Lipofactamine RNAiMAX was used to transfect siRNAs obtained from Integrated DNA Technologies (IDT).

RNA isolation and qRT–PCR. RNA was isolated using RNeasy micro kit (QIAGEN) and resuspended in 10 µl of water. SuperScript IV VILO Master Mix (ThermoFisher) was used to synthesize cDNA from 1 µg of mRNA and ezDNase was used to remove DNA after reverse transcription. Primers from IDT were used for qRT–PCR reaction using SybrGreen (ThermoFisher) to evaluate the efficiency of siRNA-mediated knockdown. *B2M* and *RPL0* were used as internal reference genes and both were found to be consistent within samples after knockdown. Quantitative RT–PCR was performed in Quantstudio3 (ThermoFisher) and relative quantitation was performed by comparative cycle number, C_t.

RNA sequencing. Agilent Bioanalyzer 2100 was used to determine RNA quality and RNA integrity number (RIN) of over 8 was observed in the samples. TruSeq RNA Library from Illumina was used to prepare mRNA library. These libraries were sequenced on Illumina HiSeq to generate 30–40 million reads per sample (Single-end 75 base pair reads) and a high Q score was observed ($Q > 30$) for the sequenced data. Alignment of reads and gene-specific analysis was performed in

Table 1 | Sequences of siRNA used for the knockdown experiments in human stromal cells

Gene name	siRNA duplex name	Duplex sequence 5′	Duplex sequence 3′
LPIN1	Hs.Ri.LPIN1.13.1	GCGUCUACUUGGAUGACCUCACAGA	GCCGCAGAUGAACCUACUGGAGUGUCU
	Hs.Ri.LPIN1.13.2	AAGCAUUUUUUGUUCAAGAAACAGA	UCUUCGUAAAAAAACAAGUUCUUUGUCU
RAC2	Hs.Ri.RAC2.13.1	CCGUGUUUGACAACUAUUCAGCCAA	GUGGCACAAACUGUUGAUAAGUCGGUU
	Hs.Ri.RAC2.13.2	GGACUUUUGCUAUUGCAAAUAGAAA	GUCCUGAAAACGAUAACGUUUAUCUUU
MGAT5	Hs.Ri.MGAT5.13.1	CUCUGACUUGUUGAGUAAUCAGUCA	GUGAGACUGAACAACUCAUUAGUCAGU
	Hs.Ri.MGAT5.13.2	CAUGACAGCUUAUGAUCUGAAGAAA	CAGUACUGUCGAAUACUAGACUUCUUU
WNT5B	Hs.Ri.WNT5B.13.1	CGGUUUCUCUCUGACAUUAAAUGCC	AUGCCAAAGAGAGACUGUAAUUUACGG
	Hs.Ri.WNT5B.13.3	GAGGAAGCUGUGCCAAUUGUACCAG	GUCUCCUUCGACACGGUUAACAUGGUC
STARD7	Hs.Ri.STARD7.13.2	GGUAUCUCACUGAGCUAAUCUGGAA	AGCCAUAGAGUGACUCGAUUAGACCUU
	Hs.Ri.STARD7.13.3	GUCCCCACAAGUCAUUUGAUGAGAA	GGCAGGGGUGUUCAGUAAACUACUCUU
YAP1	Hs.Ri.YAP1.13.1	GGUCAGAGAUACUUCUUAAAUCACA	GACCAGUCUCUAUGAAGAAUUUAGUGU
TGFB1	Hs.Ri.TGFB1.13.1	CAGCAACAAUUCCUGGCGAUACCTC	AUGUCGUUGUUAAGGACCGCUAUGGAG
	Hs.Ri.TGFB1.13.2	CUACUGUAGUUAGAUCUAUUUAUTG	GUGAUGACAUCAAUCUAGAUAAAUAAC
TGFB3	Hs.Ri.TGFB3.13.1	CAACUUAGGUCUAGAAAUCAGCATT	AGGUUGAAUCCAGAUCUUUAGUCGUAA
	Hs.Ri.TGFB3.13.2	AAGUAUGAAUAUUACUCUCAAAATC	UGUUCAUACUUAUAAUGAGAGUUUUAG
ACVR1	hs.Ri.ACVR1.13.1	GACUUUGACCAAAAUUGAUAAUUCC	UUCUGAAACUGGUUUUAACUAUUAAGG
	hs.Ri.ACVR1.13.2	CGCUACGGGGAAAAUGCAUUUUCTT	UUGCGAUGCCCCUUUUACGUAAAAGAA
Twist1	hs.Ri.TWIST1.13.1	UUCUGAUAGAAGUCUGAACAGUUGT	GUAAGACUAUCUUCAGACUUGUCAACA
	hs.Ri.TWIST1.13.2	CUAUUUUAAAAUGGUAACAAUCAGA	GAGAUAAAAUUUUACCAUUGUUAGUCU
NCOA3	hs.Ri.NCOA3.13.1	CUGCCAAUCUUAGUGAUAUUGACAA	UAGACGGUUAGAAUCACUAUAACUGUU
	hs.Ri.NCOA3.13.3	CCAGUGGAAUUGGUGAUUCUGAATT	CAGGUCACCUUAACCACUAAGACUUAA
ERBB3	hs.Ri.ERBB3.13.1	GCCAUCUUCGUCAUGUUGAACUATA	AACGGUAGAAGCAGUACAACUUGAUAU
	hs.Ri.ERBB3.13.2	CACUGUACAAGCUCUACGAGAGGTG	CUGUGACAUGUUCGAGAUGCUCUCCAC
DDR2	hs.Ri.DDR2.13.1	GUCAGUUACACCAAUCUGAAGUUTA	GACAGUCAAUGUGGUUAGACUUCAAAU
	hs.Ri.DDR2.13.3	CCACUCCAUCUGGACAUUUAAUGAA	ACGGUGAGGUAGACCUGUAAAUUACUU
BMP4	hs.Ri.BMP4.13.1	CAGUCCUUGAGGAUAGACAGAUATA	CCGUCAGGAACUCCUAUCUGUCUAUAU
	hs.Ri.BMP4.13.2	CCUUGUUUUCUGUCAAGACACCATG	ACGGAACAAAAGACAGUUCUGUGGUAC
MMP1	hs.Ri.MMP1.13.1	AGCAGACAUCAUGAUAUCUUUUGTC	GUUCGUCUGUAGUACUAUAGAAAACAG
	hs.Ri.MMP1.13.3	GUCAACCUUGUUUCUACUGUUUUAT	UUCAGUUGGAACAAAGAUGACAAAAUA
CD44	hs.Ri.CD44.13.1	GCUCUGAGCAUCGGAUUUGAGACCT	UUCGAGACUCGUAGCCUAAACUCUGGA

Partek Flow software v.5.0. Human cells data were aligned to reference genome (hg38) using STAR alignment (in Partek Flow) and bovine data were aligned using Bos Taurus assembly UMD_3.1.1/bosTau8. Quantification was performed using quantify to annotation model (Partek E/M) using Ensemble Transcripts release 85 (humans) or Ensemble-UMD3.1 gene annotation model. Normalization was performed using TPM[73]. Gene-level comparison and statistical analysis was performed using analysis of variance and significance of (adjusted) $P=0.05$ or less was considered for analysis. Gene lists comparison was performed by obtaining ontology/pathway specific list from Gene Ontology[74] or Kyoto Encyclopedia of Genes and Genomes (KEGG[75]).

Comparative transcriptome analysis. Raw sequence reads (single-ended 75 base pairs) for ESFs from rabbit (*Oryctolagus cuniculus*), rat (*Rattus norvegicus*), guinea pig (*Cavia procellus*), cat (*Felis catus*), horse (*Equus caballus*) and sheep (*Ovis aries*) were aligned to reference genome assemblies OryCun2.0, Rnor_6.0, Cavpor3.0, Felis_catus_8.0, Equcab2 and Oar_v3.1, respectively, using Tophat2 (v.2.1.1). Read counts for all genes were calculated using HTSeq (v.0.6.1p1, https://htseq.readthedocs.io/en/release_0.11.1/index.html) with Python (v.2.7) according to Ensembl gene annotation release 92 (horse) or release 89 (other species). Then TPM were calculated to estimate relative mRNA abundance[73]. To make gene expression levels comparable across species, we further normalized TPMs such that one-to-one orthologues have the same sum across species. The orthologue tables in this analysis were downloaded from Ensembl using BioMart tool. The ancestral state reconstruction for gene expression was performed on $\sqrt{\text{TPM}}$ using function 'ace' from R package 'APE'[76,77].

Two genes that have been found to influence invasibility in our knockdown experiments (Fig. 4b,c), *YAP1* and *MMP1*, have one-to-many or no orthologues in some species in our analysis. *YAP1* has two orthologues in cow, ENSBTAG00000039307 (TPM = 183.4) and ENSBTAG00000047406 (TPM = 96.3) and no orthologue in guinea pig. *MMP1* has two orthologues in cow, ENSBTAG00000015818 (TPM = 0.053) and ENSBTAG00000048029 (TPM = 0.645) and three orthologues in rat, ENSRNOG00000055895 (TPM = 0), ENSRNOG00000008881 (TPM = 0.157) and ENSRNOG00000032353 (TPM = 0.698). In these cases, the orthologues with the highest TPM were used to perform the ancestral state reconstruction.

Reporting Summary. Further information on research design is available in the Nature Research Reporting Summary linked to this article.

Data availability

Data for the human–cow transcriptome comparison with and without co-culture with trophoblast cells are available under GSE136299 in the Gene Expression Omnibus (GEO) database of NCBI, https://www.ncbi.nlm.nih.gov/geo/. The comparative fibroblast gene expression data are available under PRJNA564062 under SUB6229748 and SUB6264591 on the Sequence Read Archive (SRA) of NCBI, https://www.ncbi.nlm.nih.gov/sra.

Code availability

The computational methods are described and cited in Methods. No new code was used in this study.

Received: 21 March 2019; Accepted: 22 October 2019;
Published online: 25 November 2019

References

1. Chaturvedi, P. et al. Hypoxia-inducible factor-dependent breast cancer–mesenchymal stem cell bidirectional signaling promotes metastasis. *J. Clin. Invest.* **123**, 189–205 (2013).

2. Colegio, O. R. et al. Functional polarization of tumour-associated macrophages by tumour-derived lactic acid. *Nature* **513**, 559–563 (2014).
3. Zhang, W. & Huang, P. Cancer–stromal interactions: role in cell survival, metabolism and drug sensitivity. *Cancer Bio. Ther.* **11**, 150–156 (2011).
4. Luga, V. & Wrana, J. L. Tumor–stroma interaction: revealing fibroblast-secreted exosomes as potent regulators of Wnt–planar cell polarity signaling in cancer metastasis. *Cancer Res.* **73**, 6843–6847 (2013).
5. Murray, M. J. & Lessey, B. A. Embryo implantation and tumor metastasis: common pathways of invasion and angiogenesis. *Semin. Reprod. Endocrinol.* **17**, 275–290 (1999).
6. Ferretti, C., Bruni, L., Dangles-Marie, V., Pecking, A. P. & Bellet, D. Molecular circuits shared by placental and cancer cells, and their implications in the proliferative, invasive and migratory capacities of trophoblasts. *Hum. Reprod. Update* **13**, 121–141 (2007).
7. Ratcliffe, H. L. Incidence and nature of tumors in captive wild mammals and birds. *Cancer Res.* **17**, 132–157 (1932).
8. Canfield, P. J., Hartley, W. J. & Reddacliff, G. L. Spontaneous proliferations in Australian marsupials—a survey and review. 2. Dasyurids and bandicoots. *J. Comp. Pathol.* **103**, 147–158 (1990).
9. D'Souza, A. W. & Wagner, G. P. Malignant cancer and invasive placentation: a case for positive pleiotropy between endometrial and malignancy phenotypes. *Evol. Mes. Public Health* **2014**, 136–145 (2014).
10. Perry, J. K., Lins, R. J., Lobie, P. E. & Mitchell, M. D. Regulation of invasive growth: similar epigenetic mechanisms underpin tumour progression and implantation in human pregnancy. *Clin. Sci.* **118**, 451–457 (2009).
11. Bruning, A., Makovitzky, J., Gingelmaier, A., Friese, K. & Mylonas, I. The metastasis-associated genes MTA1 and MTA3 are abundantly expressed in human placenta and chorionic carcinoma cells. *Histochem. Cell Biol.* **132**, 33–38 (2009).
12. Wildman, D. E. et al. Evolution of the mammalian placenta revealed by phylogenetic analysis. *Proc. Natl Acad. Sci. USA* **103**, 3203–3208 (2006).
13. Mess, A. & Carter, A. M. Evolutionary transformation of fetal membrane characters in Eutheria with special reference to Afrotheria. *J. Exp. Zool. B* **306**, 140–163 (2006).
14. Elliot, M. G. & Crespi, B. J. Phylogenetic evidence for early hemochorial placentation in eutheria. *Placenta* **30**, 949–967 (2009).
15. Haeger, A., Krause, M., Wolf, K. & Friedl, P. Cell jamming: collective invasion of mesenchymal tumor cells imposed by tissue confinement. *Biochim. Biophys. Acta* **1840**, 2386–2395 (2014).
16. Shamir, E. R., Coutinho, K., Georgess, D., Auer, M. & Ewald, A. J. Twist1-positive epithelial cells retain adhesive and proliferative capacity throughout dissemination. *Biol. Open* **5**, 1216–1228 (2016).
17. Wolf, K. et al. Multi-step pericellular proteolysis controls the transition from individual to collective cancer cell invasion. *Nat. Cell Biol.* **9**, 893–904 (2007).
18. Lau, T. S. et al. A loop of cancer–stroma–cancer interaction promotes peritoneal metastasis of ovarian cancer via TNFalpha–TGFalpha–EGFR. *Oncogene* **36**, 3576–3587 (2017).
19. Bremnes, R. M. et al. The role of tumor stroma in cancer progression and prognosis: emphasis on carcinoma-associated fibroblasts and non-small cell lung cancer. *J. Thorac. Oncol.* **6**, 209–217 (2011).
20. Howard, J. D. et al. Notch signaling mediates melanoma–endothelial cell communication and melanoma cell migration. *Pigment Cell Melanoma Res.* **26**, 697–707 (2013).
21. Kshitiz, Afzal, J., Kim, S. Y. & Kim, D. H. A nanotopography approach for studying the structure–function relationships of cells and tissues. *Cell Adh. Migr.* **9**, 300–307 (2015).
22. Kim, D. H., Provenzano, P. P., Smith, C. L. & Levchenko, A. Matrix nanotopography as a regulator of cell function. *J. Cell Biol.* **197**, 351–360 (2012).
23. Kondo, F. Assessment of stromal invasion for correct histological diagnosis of early hepatocellular carcinoma. *Int. J. Hepatol.* **2011**, 241652 (2011).
24. Khalil, A. A. et al. Collective invasion in ductal and lobular breast cancer associates with distant metastasis. *Clin. Exp. Metastasis* **34**, 421–429 (2017).
25. Friedl, P. & Alexander, S. Cancer invasion and the microenvironment: plasticity and reciprocity. *Cell* **147**, 992–1009 (2011).
26. Cheung, K. J. et al. Polyclonal breast cancer metastases arise from collective dissemination of keratin 14-expressing tumor cell clusters. *Proc. Natl Acad. Sci. USA* **113**, E854–863 (2016).
27. Ramsey, E. M. *The Placenta: Human and Animal* (Praeger, 1982).
28. Wooding, P. & Burton, G. *Comparative Placentation: Structures, Functions and Evolution* (Springer, 2008).
29. Orendi, K. et al. Placental and trophoblastic in vitro models to study preventive and therapeutic agents for preeclampsia. *Placenta* **32**, S49–54 (2011).
30. Bertero, L. et al. Eighth Edition of the UICC Classification of Malignant Tumours: an overview of the changes in the pathological TNM classification criteria—what has changed and why? *Virchows Arch.* **472**, 519–531 (2018).
31. Musser, J. M. & Wagner, G. P. Character trees from transcriptome data: origin and individuation of morphological characters and the so-called "species signal". *J. Exp. Zool. B* **324**, 588–604 (2015).
32. Wagner, G. P. *Homology, Genes and Evolutionary Innovation* (Princeton Univ. Press, 2014).
33. Liang, C., Musser, J. M., Cloutier, A., Prum, R. O. & Wagner, G. P. Pervasive correlated evolution in gene expression shapes cell and tissue type transcriptomes. *Genome Biol. Evol.* **10**, 538–552 (2018).
34. Garma-Avina, A., Valli, V. E. & Lumsden, J. H. Cutaneous melanomas in domestic animals. *J. Cutan. Pathol.* **8**, 3–24 (1981).
35. Meng, X. M., Nikolic-Paterson, D. J. & Lan, H. Y. TGF-beta: the master regulator of fibrosis. *Nat. Rev. Nephrol.* **12**, 325–338 (2016).
36. Guido, C. et al. Metabolic reprogramming of cancer-associated fibroblasts by TGF-beta drives tumor growth: connecting TGF-beta signaling with "Warburg-like" cancer metabolism and L-lactate production. *Cell Cycle* **11**, 3019–3035 (2012).
37. Vallee, A., Lecarpentier, Y., Guillevin, R. & Vallee, J. N. Interactions between TGF-beta1, canonical WNT/beta-catenin pathway and PPAR gamma in radiation-induced fibrosis. *Oncotarget* **8**, 90579–90604 (2017).
38. Calon, A. et al. Stromal gene expression defines poor-prognosis subtypes in colorectal cancer. *Nat. Genet.* **47**, 320–329 (2015).
39. Piersma, B., Bank, R. A. & Boersema, M. Signaling in fibrosis: TGF-beta, WNT, and YAP/TAZ Converge. *Front. Med.* **2**, 59 (2015).
40. Akhmetshina, A. et al. Activation of canonical Wnt signalling is required for TGF-beta-mediated fibrosis. *Nat. Commun.* **3**, 735 (2012).
41. Menke, J. et al. Circulating CSF-1 promotes monocyte and macrophage phenotypes that enhance lupus nephritis. *J. Am. Soc. Nephrol.* **20**, 2581–2592 (2009).
42. Takada, I., Kouzmenko, A. P. & Kato, S. Wnt and PPARgamma signaling in osteoblastogenesis and adipogenesis. *Nat. Rev. Rheumatol.* **5**, 442–447 (2009).
43. Ahn, E. H. et al. Spatial control of adult stem cell fate using nanotopographic cues. *Biomaterials* **35**, 2401–2410 (2014).
44. Hubbi, M. E. et al. A nontranscriptional role for HIF-1alpha as a direct inhibitor of DNA replication. *Sci. Signal.* **6**, ra10 (2013).
45. Suhail, Y. et al. Modeling intercellular transfer of biomolecules through tunneling nanotubes. *Bull. Math. Biol.* **75**, 1400–1416 (2013).
46. Zhang, P., Takeuchi, K., Csaki, L. S. & Reue, K. Lipin-1 phosphatidic phosphatase activity modulates phosphatidate levels to promote peroxisome proliferator-activated receptor gamma (PPARgamma) gene expression during adipogenesis. *J. Biol. Chem.* **287**, 3485–3494 (2012).
47. Park, H. W. et al. Alternative Wnt signaling activates YAP/TAZ. *Cell* **162**, 780–794 (2015).
48. Meredith, R. W. et al. Impacts of the cretaceous terrestrial revolution and KPg extinction on mammal diversification. *Science* **334**, 521–524 (2011).
49. de Magalhaes, J. P. & Costa, J. A database of vertebrate longevity records and their relation to other life-history traits. *J. Evol. Biol.* **22**, 1770–1774 (2009).
50. Seluanov, A. et al. Hypersensitivity to contact inhibition provides a clue to cancer resistance of naked mole-rat. *Proc. Natl Acad. Sci. USA* **106**, 19352–19357 (2009).
51. Tian, X. et al. High-molecular-mass hyaluronan mediates the cancer resistance of the naked mole rat. *Nature* **499**, 346–349 (2013).
52. Nunney, L. Lineage selection and the evolution of multistage carcinogenesis. *Proc. Biol. Sci.* **266**, 493–498 (1999).
53. Caulin, A. F., Graham, T. A., Wang, L. S. & Maley, C. C. Solutions to Peto's paradox revealed by mathematical modelling and cross-species cancer gene analysis. *Phil. Trans. R. Soc. Lond. B* **370**, 20140222 (2015).
54. Abegglen, L. M. et al. Potential mechanisms for cancer resistance in elephants and comparative cellular response to DNA damage in humans. *J. Am. Med. Assoc.* **314**, 1850–1860 (2015).
55. Sulak, M. et al. TP53 copy number expansion is associated with the evolution of increased body size and an enhanced DNA damage response in elephants. *eLife* **5**, e11994 (2016).
56. Costanzo, V., Bardelli, A., Siena, S. & Abrignani, S. Exploring the links between cancer and placenta development. *Open Biol.* **8**, 180081 (2018).
57. Curik, I. et al. Inbreeding and melanoma in Lipizzan horses. *Agric. Conspec. Sci.* **65**, 181–186 (2000).
58. Pandey, M. K. et al. Benign melanocytoma in a non-descript cow: a case report. *Indian J. Anim. Res.* **50**, 632–633 (2016).
59. Priester, W. A. & Mantel, N. Occurrence of tumors in domestic animals. Data from 12 United States and Canadian colleges of veterinary medicine. *J. Nat. Cancer Inst.* **47**, 1333–1344 (1971).
60. Bego, T. et al. Association of PPARG and LPIN1 gene polymorphisms with metabolic syndrome and type 2 diabetes. *Med. Glas.* **8**, 76–83 (2011).
61. Wong, N. A. & Pignatelli, M. Beta-catenin—a linchpin in colorectal carcinogenesis? *Am. J. Pathol.* **160**, 389–401 (2002).
62. Zhao, B., Li, L., Lei, Q. & Guan, K. L. The Hippo–YAP pathway in organ size control and tumorigenesis: an updated version. *Genes Dev.* **24**, 862–874 (2010).
63. Padua, D. & Massague, J. Roles of TGFbeta in metastasis. *Cell Res.* **19**, 89–102 (2009).

64. Wendt, M. K., Tian, M. & Schiemann, W. P. Deconstructing the mechanisms and consequences of TGF-beta-induced EMT during cancer progression. *Cell Tissue Res.* **347**, 85–101 (2012).
65. Weeraratna, A. T. et al. Wnt5a signaling directly affects cell motility and invasion of metastatic melanoma. *Cancer Cell* **1**, 279–288 (2002).
66. Kurayoshi, M. et al. Expression of Wnt-5a is correlated with aggressiveness of gastric cancer by stimulating cell migration and invasion. *Cancer Res.* **66**, 10439–10448 (2006).
67. Kim, J. Y., Kim, G., Lim, S. C. & Choi, H. S. LPIN1 promotes epithelial cell transformation and mammary tumourigenesis via enhancing insulin receptor substrate 1 stability. *Carcinogenesis* **37**, 1199–1209 (2016).
68. Mendelsohn, R. et al. Complex *N*-glycan and metabolic control in tumor cells. *Cancer Res.* **67**, 9771–9780 (2007).
69. Carter, A. M. Evolution of placental function in mammals: the molecular basis of gas and nutrient transfer, hormone secretion, and immune responses. *Physiol. Rev.* **92**, 1543–1576 (2012).
70. Kirkun, G. et al. A novel immortalized human endometrial stroma cell line with normal progestational response. *Endocrinology* **145**, 2291–2296 (2004).
71. Haeger, J. D., Hambruch, N., Dilly, M., Froehlich, R. & Pfarrer, C. Formation of bovine placental trophoblast spheroids. *Cells Tissues Organs* **193**, 274–284 (2011).
72. Hambruch, N., Haeger, J. D., Dilly, M. & Pfarrer, C. EGF stimulates proliferation in the bovine placental trophoblast cell line F3 via Ras and MAPK. *Placenta* **31**, 67–74 (2010).
73. Wagner, G. P., Kin, K. & Lynch, V. J. Measurement of mRNA abundance using RNA-seq data: RPKM measure is inconsistent among samples. *Theory Biosci.* **131**, 281–285 (2012).
74. The Gene Ontology Consortium The gene ontology resource: 20 years and still GOing strong. *Nucleic Acids Res.* **47**, D330–D338 (2019).
75. Kanehisa, M. & Goto, S. KEGG: Kyoto encyclopedia of genes and genomes. *Nucleic Acids Res.* **28**, 27–30 (2000).
76. Paradis, E., Claude, J. & Strimmer, K. APE: Analyses of phylogenetics and evolution in R language. *Bioinformatics* **20**, 289–290 (2004).
77. Paradis, E. *Analysis of Phylogenetics and Evolution with R* 2nd edn (Springer, 2012).

Acknowledgements

This work was funded by National Cancer Institute Center grant no. U54-CA209992.

Author contributions

G.P.W. and A.L. conceptualized this project. K., J.D.M. and C.L. were responsible for data curation. K., C.L. and G.P.W. conducted the formal analysis. A.L. and G.P.W. acquired the funding. K., E.E., J.D.M. and A.H. undertook the investigation. K. and H.N.K. were responsible for the methodology. A.L. and G.P.W. were responsible for project admininstration. J.-D.H., C.P., T.H., T.O., T.S., M.P. and D.F.A. obtained resources. C.L. worked on software. G.P.W. and A.L. supervised the project. K., E.M.E. and G.P.W. validated the results. K. and C.L. worked on visualization. K., G.P.W. and A.L. wrote the first draft and all other authors were involved in reviewing and editing.

Competing interests

The authors declare no competing interests.

Additional information

Extended data is available for this paper at https://doi.org/10.1038/s41559-019-1046-4.

Supplementary information is available for this paper at https://doi.org/10.1038/s41559-019-1046-4.

Correspondence and requests for materials should be addressed to K., A.L. or G.P.W.

Reprints and permissions information is available at www.nature.com/reprints.

Publisher's note Springer Nature remains neutral with regard to jurisdictional claims in published maps and institutional affiliations.

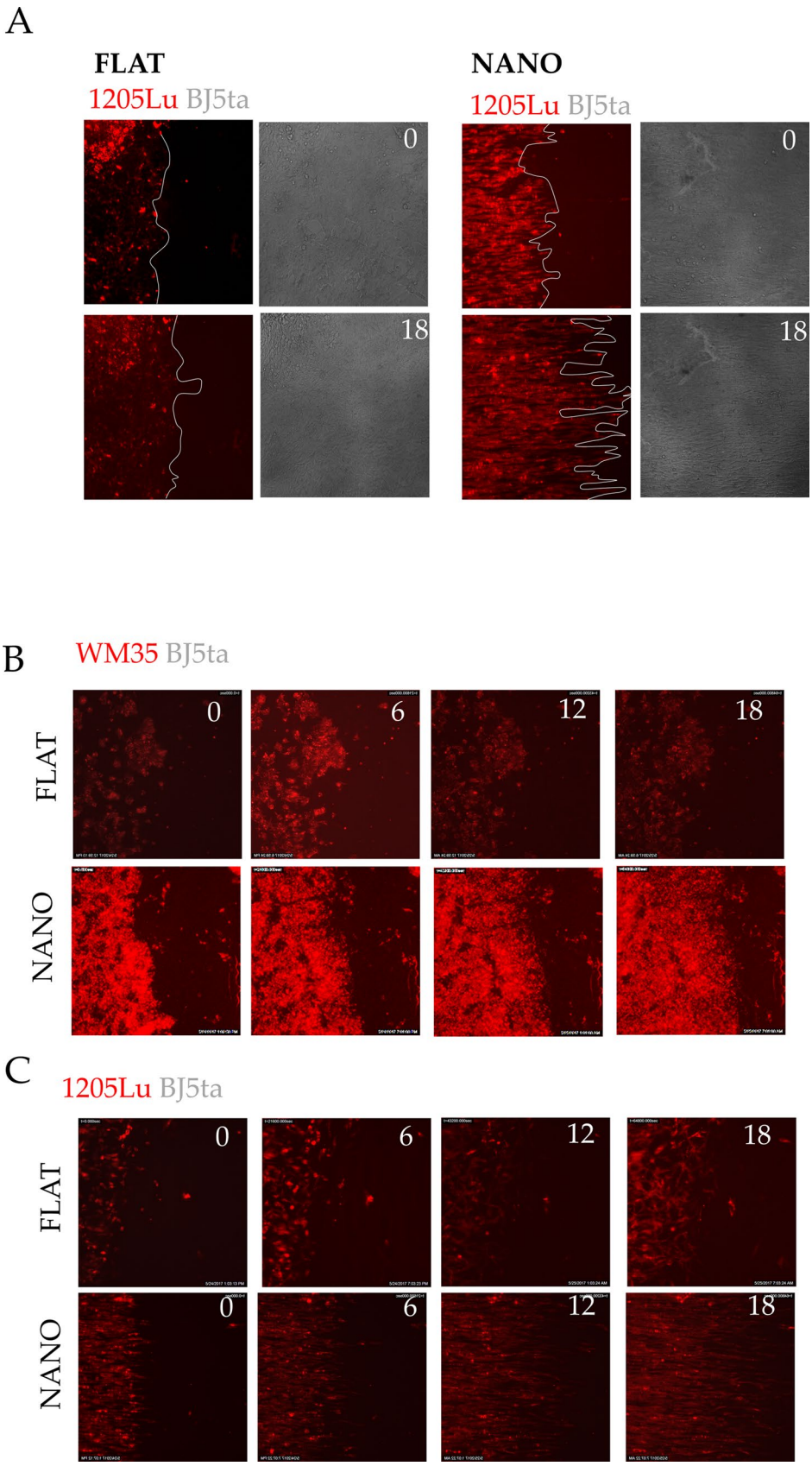

Extended Data Fig. 1 | Nanotextured stromal invasion assay quantitatively and sensitively measures collective intrusion of cells into stroma. (A) Time stamped images at 0 and 18 hours showing extent of invasion by DiI-labelled 1205Lu cells (red) into BJ5ta stromal fibroblast monolayer (unlabelled) on flat and nanotextured substrata; Quantification shown in Fig. 1d. (B-C) Sensitive measurement of differences in invasion by nanotextured stromal invasion platform; Time stamped images at 0, 6, 12 and 18 hours showing extent of invasion by DiI-labelled non-malignant WM35 (B), and malignant 1205Lu (C) cells into BJ5ta monolayer shown in both flat, and nanotextured cell patterned assay; Quantification shown in Fig. 1e.

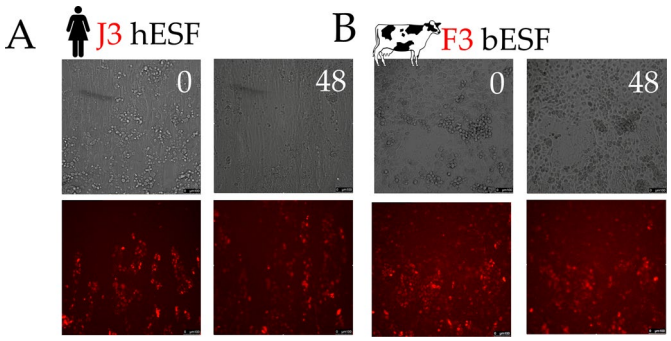

Extended Data Fig. 2 | Human and bovine trophoblasts exhibit different invasive potential into endometrial stroma. Time stamped images showing extent of invasion of human choriocarcinoma-derived trophoblasts, J3 (red) (A), and bovine trophoblasts, F3 (red) (B) into their respective endometrial stromal fibroblast monolayers at 0, and 48 hours.

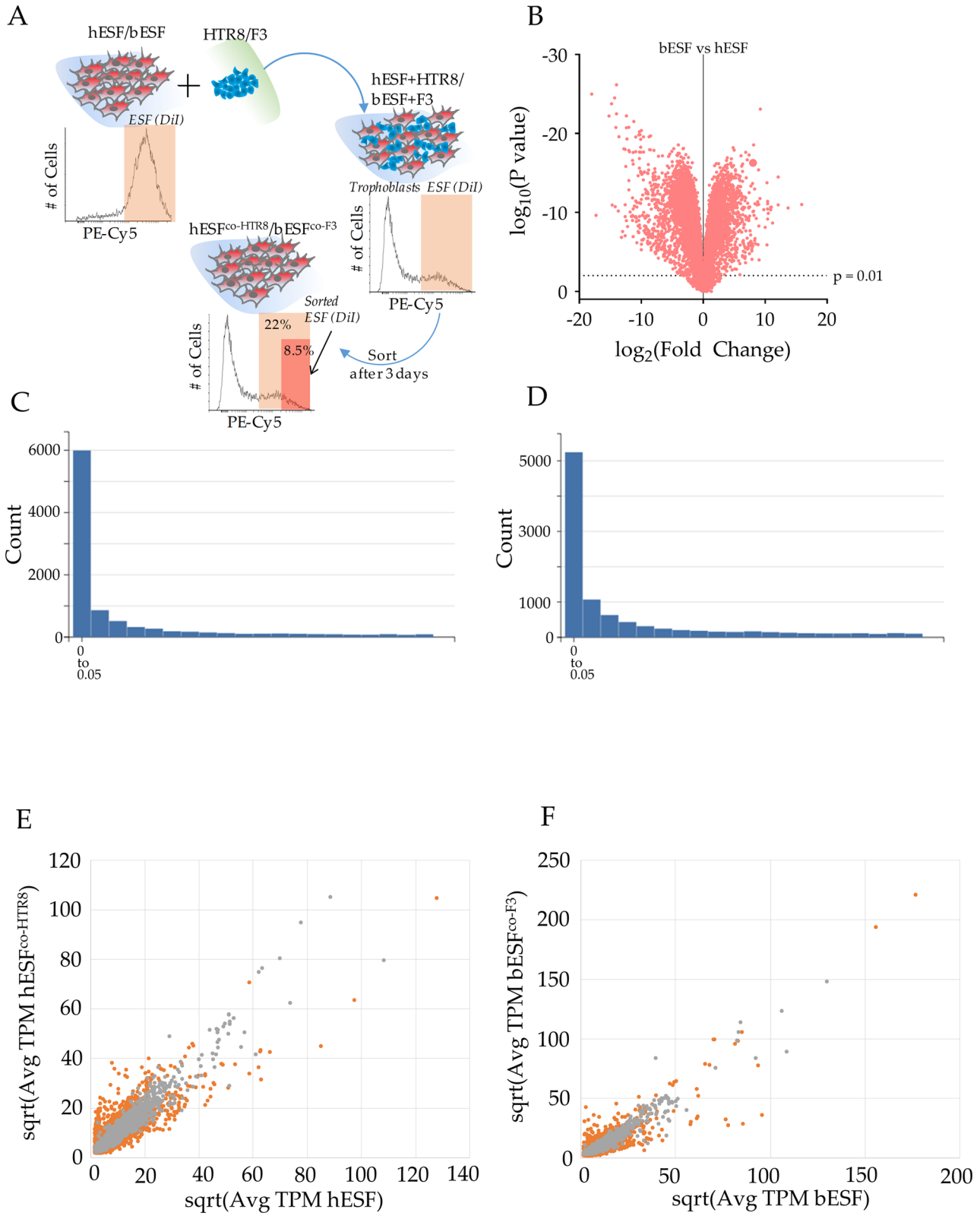

Extended Data Fig. 3 | Human and bovine ESFs respond differently to co-culture with trophoblasts. (A) Experimental plan to isolate endometrial cells after co-culture with respective trophoblast; (B) Volcano plot showing fold change in genes between bovine versus human endometrial stromal fibroblasts, along with their significance depicted in P value. (C) P-value distribution of t-tests comparing human ESFs with and without co-culture with HTR8 trophoblast cells. (D) P-value distribution of t-tests comparing bovine ESFs with and without co-culture with F3 trophoblast cells. In both C and D, note that thin right hand tail of the distribution, which indicates that a large number of genes are differentially expressed in response to the presence of the corresponding trophoblast cells. (E-F) Scatter plots showing relative TPM values of genes between (E) hESF and hESF co-cultured with HTR8, and (F) bESF and bESF co-cultured with F3; Red dots refer to individual gene transcripts abundance significantly different in between the compared conditions.

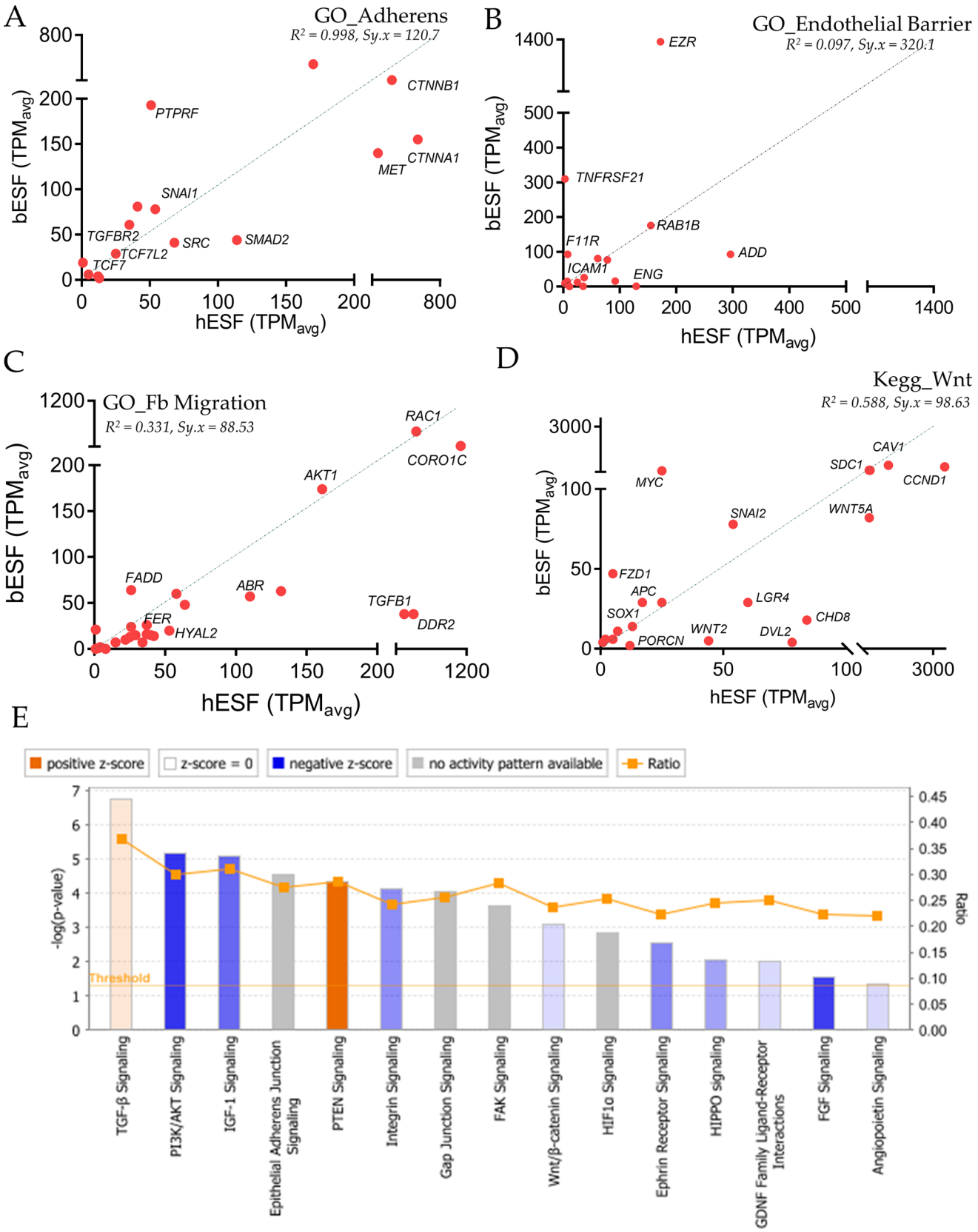

Extended Data Fig. 4 | Human and bovine endometrial stromal fibroblasts do not appear to differentially respond to their respective trophoblasts by regulating cell-cell adhesion. Gene ontology analysis of individual genes belonging to GO_Adherens (A), GO_Endothelial Barrier (B), GO_Fibroblast Migration (C), and Kegg ontology for Wnt Signalling (D) for hESF and bESF shown with their relative TPM values; Also are shown the coefficient of determinant, R^2 for the linear regression between TPM values of hESF and bESF in a given gene-sets, along with the standard deviation of the residuals, Sy.x. (E) Ingenuity Pathway Analysis of selected signalling pathways differentially activated in hESF and bESF; Shown are –log(p-values) of genes in the respective pathways differentially activated, while the colour depicts the z-score.

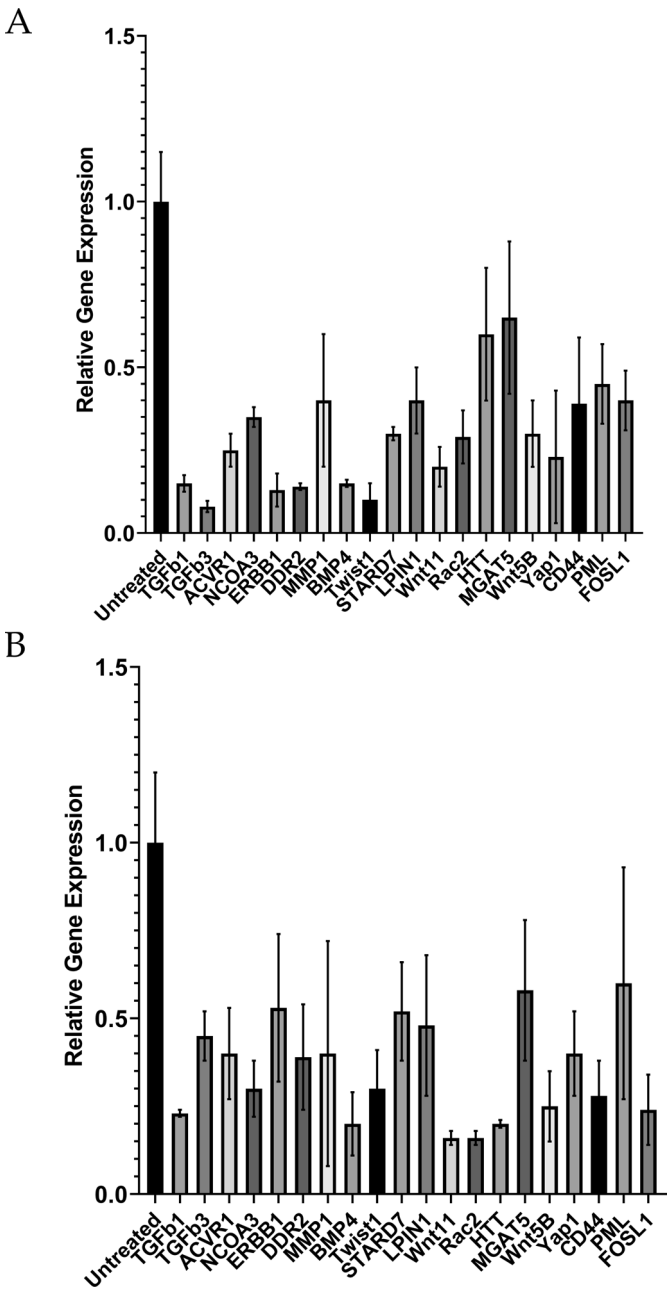

Extended Data Fig. 5 | siRNA-induced gene knockdown reduces transcript levels in hESFs and BJ5ta cells. qRT–PCR results showing the percentage knockdown of transcript levels in hESF (A) and BJ5ta (B), calculated using $\Delta\Delta C_t$ method, compared using GAPDH as housekeeping gene with scrambled siRNA as control. For both A, and B, n = 4 biological replicates.

nature research

Corresponding author(s): Günter P. Wagner
Kshitiz Kz
Andre Levchenko

Last updated by author(s): 2019/03/27

Reporting Summary

Nature Research wishes to improve the reproducibility of the work that we publish. This form provides structure for consistency and transparency in reporting. For further information on Nature Research policies, see Authors & Referees and the Editorial Policy Checklist.

Statistics

For all statistical analyses, confirm that the following items are present in the figure legend, table legend, main text, or Methods section.

n/a	Confirmed	
☐	☒	The exact sample size (*n*) for each experimental group/condition, given as a discrete number and unit of measurement
☐	☒	A statement on whether measurements were taken from distinct samples or whether the same sample was measured repeatedly
☐	☒	The statistical test(s) used AND whether they are one- or two-sided *Only common tests should be described solely by name; describe more complex techniques in the Methods section.*
☐	☒	A description of all covariates tested
☐	☒	A description of any assumptions or corrections, such as tests of normality and adjustment for multiple comparisons
☐	☒	A full description of the statistical parameters including central tendency (e.g. means) or other basic estimates (e.g. regression coefficient) AND variation (e.g. standard deviation) or associated estimates of uncertainty (e.g. confidence intervals)
☐	☒	For null hypothesis testing, the test statistic (e.g. *F*, *t*, *r*) with confidence intervals, effect sizes, degrees of freedom and *P* value noted *Give P values as exact values whenever suitable.*
☒	☐	For Bayesian analysis, information on the choice of priors and Markov chain Monte Carlo settings
☒	☐	For hierarchical and complex designs, identification of the appropriate level for tests and full reporting of outcomes
☒	☐	Estimates of effect sizes (e.g. Cohen's *d*, Pearson's *r*), indicating how they were calculated

Our web collection on statistics for biologists contains articles on many of the points above.

Software and code

Policy information about availability of computer code

Data collection	QuantStudio Software V1.3 (qRT-PCR),
Data analysis	Partek® Flow® software, version 5.0 was used to analyze the RNA sequencing data. Fiji Image Analysis Software was used for Image analysis. Expression suite software was used for qRT-PCR. GraphPad Prism was used for the other statistical analysis

For manuscripts utilizing custom algorithms or software that are central to the research but not yet described in published literature, software must be made available to editors/reviewers. We strongly encourage code deposition in a community repository (e.g. GitHub). See the Nature Research guidelines for submitting code & software for further information.

Data

Policy information about availability of data

All manuscripts must include a data availability statement. This statement should provide the following information, where applicable:

- Accession codes, unique identifiers, or web links for publicly available datasets
- A list of figures that have associated raw data
- A description of any restrictions on data availability

The data generated that supports this study will be available from the corresponding author upon request.

Field-specific reporting

Please select the one below that is the best fit for your research. If you are not sure, read the appropriate sections before making your selection.

☒ Life sciences ☐ Behavioural & social sciences ☐ Ecological, evolutionary & environmental sciences

Life sciences study design

All studies must disclose on these points even when the disclosure is negative.

Sample size	For each invasion study, at least 6 (or up to 10) samples were chosen for a live/ end-point study.
Data exclusions	All samples were included in the final analysis, except those in which the cell layers ripped off during image acquisition. This occurred not due to the biological samples, but because of the swelling of the underlying nanopatterns due to manual plasma treatment.
Replication	All experiments were repeated at least 3 times.
Randomization	This was not relevant to our study.
Blinding	All experiments were analyzed by undergraduate assistants, who were not aware of the actual conditions. The analyses are objective, but were separated from the person performing image acquisition.

Reporting for specific materials, systems and methods

We require information from authors about some types of materials, experimental systems and methods used in many studies. Here, indicate whether each material, system or method listed is relevant to your study. If you are not sure if a list item applies to your research, read the appropriate section before selecting a response.

Materials & experimental systems

n/a	Involved in the study
☐	☐ Antibodies
☐	☒ Eukaryotic cell lines
☐	☐ Palaeontology
☐	☐ Animals and other organisms
☐	☐ Human research participants
☐	☐ Clinical data

Methods

n/a	Involved in the study
☐	☐ ChIP-seq
☐	☐ Flow cytometry
☐	☐ MRI-based neuroimaging

Antibodies

Antibodies used	*Describe all antibodies used in the study; as applicable, provide supplier name, catalog number, clone name, and lot number.*
Validation	*Describe the validation of each primary antibody for the species and application, noting any validation statements on the manufacturer's website, relevant citations, antibody profiles in online databases, or data provided in the manuscript.*

Eukaryotic cell lines

Policy information about cell lines

Cell line source(s)	BJ5ta (ATCC), HTR8/SVNeo (ATCC)
Authentication	The cell lines were not authenticated separately, it was bought from ATCC and directly used for this study within a few months. HTR8 was a newly available cell line in ATCC, and we waited for its initial authentication from ATCC.
Mycoplasma contamination	Cell lines tested negative for mycoplasma.
Commonly misidentified lines (See ICLAC register)	*Name any commonly misidentified cell lines used in the study and provide a rationale for their use.*

Palaeontology

Specimen provenance	*Provide provenance information for specimens and describe permits that were obtained for the work (including the name of the issuing authority, the date of issue, and any identifying information).*
Specimen deposition	*Indicate where the specimens have been deposited to permit free access by other researchers.*

Dating methods	*If new dates are provided, describe how they were obtained (e.g. collection, storage, sample pretreatment and measurement), where they were obtained (i.e. lab name), the calibration program and the protocol for quality assurance OR state that no new dates are provided.*

☐ Tick this box to confirm that the raw and calibrated dates are available in the paper or in Supplementary Information.

Animals and other organisms

Policy information about studies involving animals; ARRIVE guidelines recommended for reporting animal research

Laboratory animals	*For laboratory animals, report species, strain, sex and age OR state that the study did not involve laboratory animals.*
Wild animals	*Provide details on animals observed in or captured in the field; report species, sex and age where possible. Describe how animals were caught and transported and what happened to captive animals after the study (if killed, explain why and describe method; if released, say where and when) OR state that the study did not involve wild animals.*
Field-collected samples	*For laboratory work with field-collected samples, describe all relevant parameters such as housing, maintenance, temperature, photoperiod and end-of-experiment protocol OR state that the study did not involve samples collected from the field.*
Ethics oversight	*Identify the organization(s) that approved or provided guidance on the study protocol, OR state that no ethical approval or guidance was required and explain why not.*

Note that full information on the approval of the study protocol must also be provided in the manuscript.

Human research participants

Policy information about studies involving human research participants

Population characteristics	*Describe the covariate-relevant population characteristics of the human research participants (e.g. age, gender, genotypic information, past and current diagnosis and treatment categories). If you filled out the behavioural & social sciences study design questions and have nothing to add here, write "See above."*
Recruitment	*Describe how participants were recruited. Outline any potential self-selection bias or other biases that may be present and how these are likely to impact results.*
Ethics oversight	*Identify the organization(s) that approved the study protocol.*

Note that full information on the approval of the study protocol must also be provided in the manuscript.

Clinical data

Policy information about clinical studies

All manuscripts should comply with the ICMJE guidelines for publication of clinical research and a completed CONSORT checklist must be included with all submissions.

Clinical trial registration	*Provide the trial registration number from ClinicalTrials.gov or an equivalent agency.*
Study protocol	*Note where the full trial protocol can be accessed OR if not available, explain why.*
Data collection	*Describe the settings and locales of data collection, noting the time periods of recruitment and data collection.*
Outcomes	*Describe how you pre-defined primary and secondary outcome measures and how you assessed these measures.*

ChIP-seq

Data deposition

☐ Confirm that both raw and final processed data have been deposited in a public database such as GEO.

☐ Confirm that you have deposited or provided access to graph files (e.g. BED files) for the called peaks.

Data access links *May remain private before publication.*	*For "Initial submission" or "Revised version" documents, provide reviewer access links. For your "Final submission" document, provide a link to the deposited data.*
Files in database submission	*Provide a list of all files available in the database submission.*
Genome browser session (e.g. UCSC)	*Provide a link to an anonymized genome browser session for "Initial submission" and "Revised version" documents only, to enable peer review. Write "no longer applicable" for "Final submission" documents.*

Methodology

Replicates	*Describe the experimental replicates, specifying number, type and replicate agreement.*

Sequencing depth	*Describe the sequencing depth for each experiment, providing the total number of reads, uniquely mapped reads, length of reads and whether they were paired- or single-end.*
Antibodies	*Describe the antibodies used for the ChIP-seq experiments; as applicable, provide supplier name, catalog number, clone name, and lot number.*
Peak calling parameters	*Specify the command line program and parameters used for read mapping and peak calling, including the ChIP, control and index files used.*
Data quality	*Describe the methods used to ensure data quality in full detail, including how many peaks are at FDR 5% and above 5-fold enrichment.*
Software	*Describe the software used to collect and analyze the ChIP-seq data. For custom code that has been deposited into a community repository, provide accession details.*

Flow Cytometry

Plots

Confirm that:

☒ The axis labels state the marker and fluorochrome used (e.g. CD4-FITC).

☒ The axis scales are clearly visible. Include numbers along axes only for bottom left plot of group (a 'group' is an analysis of identical markers).

☐ All plots are contour plots with outliers or pseudocolor plots.

☒ A numerical value for number of cells or percentage (with statistics) is provided.

Methodology

Sample preparation	Fibroblasts were labeled with DiI and mixed with trophoblasts, and separated based on fluorescence.
Instrument	BD FACSAria II
Software	BD FacsDIVA
Cell population abundance	The cell population isolated was > 25%
Gating strategy	Gating strategy is described in the figure. In brief, we were very conservative in selecting only DiI(hi) cells.

☒ Tick this box to confirm that a figure exemplifying the gating strategy is provided in the Supplementary Information.

Magnetic resonance imaging

Experimental design

Design type	*Indicate task or resting state; event-related or block design.*
Design specifications	*Specify the number of blocks, trials or experimental units per session and/or subject, and specify the length of each trial or block (if trials are blocked) and interval between trials.*
Behavioral performance measures	*State number and/or type of variables recorded (e.g. correct button press, response time) and what statistics were used to establish that the subjects were performing the task as expected (e.g. mean, range, and/or standard deviation across subjects).*

Acquisition

Imaging type(s)	*Specify: functional, structural, diffusion, perfusion.*
Field strength	*Specify in Tesla*
Sequence & imaging parameters	*Specify the pulse sequence type (gradient echo, spin echo, etc.), imaging type (EPI, spiral, etc.), field of view, matrix size, slice thickness, orientation and TE/TR/flip angle.*
Area of acquisition	*State whether a whole brain scan was used OR define the area of acquisition, describing how the region was determined.*

Diffusion MRI ☐ Used ☐ Not used

Preprocessing

Preprocessing software

Provide detail on software version and revision number and on specific parameters (model/functions, brain extraction, segmentation, smoothing kernel size, etc.).

Normalization

If data were normalized/standardized, describe the approach(es): specify linear or non-linear and define image types used for transformation OR indicate that data were not normalized and explain rationale for lack of normalization.

Normalization template

Describe the template used for normalization/transformation, specifying subject space or group standardized space (e.g. original Talairach, MNI305, ICBM152) OR indicate that the data were not normalized.

Noise and artifact removal

Describe your procedure(s) for artifact and structured noise removal, specifying motion parameters, tissue signals and physiological signals (heart rate, respiration).

Volume censoring

Define your software and/or method and criteria for volume censoring, and state the extent of such censoring.

Statistical modeling & inference

Model type and settings

Specify type (mass univariate, multivariate, RSA, predictive, etc.) and describe essential details of the model at the first and second levels (e.g. fixed, random or mixed effects; drift or auto-correlation).

Effect(s) tested

Define precise effect in terms of the task or stimulus conditions instead of psychological concepts and indicate whether ANOVA or factorial designs were used.

Specify type of analysis: ☐ Whole brain ☐ ROI-based ☐ Both

Statistic type for inference
(See Eklund et al. 2016)

Specify voxel-wise or cluster-wise and report all relevant parameters for cluster-wise methods.

Correction

Describe the type of correction and how it is obtained for multiple comparisons (e.g. FWE, FDR, permutation or Monte Carlo).

Models & analysis

n/a	Involved in the study
☐	☐ Functional and/or effective connectivity
☐	☐ Graph analysis
☐	☐ Multivariate modeling or predictive analysis

Functional and/or effective connectivity

Report the measures of dependence used and the model details (e.g. Pearson correlation, partial correlation, mutual information).

Graph analysis

Report the dependent variable and connectivity measure, specifying weighted graph or binarized graph, subject- or group-level, and the global and/or node summaries used (e.g. clustering coefficient, efficiency, etc.).

Multivariate modeling and predictive analysis

Specify independent variables, features extraction and dimension reduction, model, training and evaluation metrics.